Supplementary Feedforward Voltage Control in a Reconfigurable Distribution Network using Robust Optimization

Jae-Young Park, *Student Member, IEEE*, Jaepil Ban, *Member, IEEE*, Young-Jin Kim, *Senior Member, IEEE*, and João P. S. Catalão, *Fellow, IEEE*

***Abstract*—Network reconfiguration (NR) has attracted much attention due to its ability to convert conventional distribution networks (DNs) into self-healing grids. This paper proposes a new strategy for real-time voltage regulation (VR) in a reconfigurable DN, whereby optimal feedforward control of distributed generators (DGs) is achieved in coordination with the operation of line switches (SWs). This enables preemptive compensation of upcoming deviations in DN voltages resulting from NR-aided load restoration. A robust optimization problem is formulated using a dynamic analytical model of NR to design the feedforward voltage controllers (FVCs) that minimize voltage deviations with respect to the H_∞ norm. Errors in the estimates of DG modeling parameters and load demands are reflected in the design of optimal FVCs via polytopic uncertainty modeling. Small-signal analysis and case studies are conducted, verifying the effectiveness and robustness of the optimal FVCs in improving real-time VR when NR is activated for load restoration. The performance of the proposed FVCs is confirmed under various conditions of a self-healing DN, characterized by network islanding and size, parameter errors, SW operations, and communication time delays.**

***Index Terms*—Load restoration, network reconfiguration, polytopic uncertainty, robust optimization, voltage control.**

NOMENCLATURE

Sets

d, q	subscripts for d- and q-axis variables
i, k, n, v	indices for SGs, IGs, buses, and vertices
t, T	index and total number of sampling time steps
G, L, N, V	total numbers of SGs, IGs, buses, and vertices
$\mathcal{P}$	convex polytope set
$\|\|\bullet\|\|_\infty$, $\|\|\bullet\|\|_2$	infinity- and two-norm values of •
$\bar{\bullet}$, $\underline{\bullet}$	maximum and minimum estimates of •
$diag(\bullet)$	block diagonal matrix composed of •
$tr(\bullet)$	sum of the diagonal elements of •
$Co(\bullet)$	convex hull for the set of vertices of •
$\sigma(\bullet)$	singular values of •

Matrices, vectors, and scalars

$u(t)$	NR-initiating signal
$H_i(s)$, $M_k(s)$	transfer functions of the FVCs for SG unit i and IG unit k
K_A, L_f	exciter amplifier gain and line filter inductance
S_L, S_r	total load demand and the amount of load to be restored
T_d	communication time delay
U_{SGi}, U_{IGk}	output signals of the FVCs for SG unit i and IG unit k
V_{SGi}, V_{IGk}	terminal voltage magnitudes of SG unit i and IG unit k
ΔT_{set}	settling time of voltage deviation
ΔV_{rms}, ΔV_{pk}	rms and peak-to-peak voltage deviations
γ	upper bound of the energy of FVC output signals
$\mathbf{d}(s)$	Padé approximation of the time-delay transfer function
$\mathbf{A_{DN}}$, $\mathbf{B_{NR}}$, $\mathbf{B_{DG}}$, $\mathbf{C_{DG}}$	modeling coefficients of a reconfigurable network
$\mathbf{A_{FF}}$, $\mathbf{B_{FF}}$, $\mathbf{C_{FF}}$, $\mathbf{U_{FF}}$	control parameters and output signals of FVCs
$\mathbf{A_{OD}}$, $\mathbf{B_{OD}}$, $\mathbf{C_{OD}}$	coefficients for the overall dynamics of a reconfigurable network including SGs and IGs with optimal FVCs
$\mathbf{G}(s)$, $\mathbf{G_d}(s)$	dynamic responses of $\mathbf{V_{DG}}$ to NR without and with consideration of communication time delays
$\mathbf{G_{FF}}(s)$	dynamic response of FVCs to an NR-initiating signal
$\mathbf{I_0}$, $\mathbf{V_0}$	dq-axis currents and voltages in the steady state
$\mathbf{I_{DG}}$, $\mathbf{I_L}$	injection currents of DGs and voltage-dependent loads
$\mathbf{\Delta I_T}$, $\mathbf{\Delta Y}$	variations in injection currents and the admittance matrix
$\mathbf{V_{DG}}$	terminal voltage magnitudes of SGs and IGs
$\mathbf{X_{DN}}$, $\mathbf{X_{FF}}$, $\mathbf{X_{OD}}$,	states of a reconfigurable network, optimal FVCs, and their overall dynamics
$\mathbf{X_{SG\mathit{i}}}$, $\mathbf{X_{IG\mathit{k}}}$	states of SG unit i and IG unit k
$\mathbf{Y_B}$, $\mathbf{Y_A}$	admittance matrices before and after NR
$\mathcal{J}$, $\mathcal{C}_{1\text{–}3}$, $\mathcal{C}_N$	objective function and constraints of an optimization problem to design optimal FVCs
$\mathbf{Q}$, $\mathcal{R}$, $\mathcal{N}$, $\mathcal{U}$, $\mathcal{V}$, $\mathcal{L}_{1\text{–}5}$	positive definite matrix for the Lyapunov condition and auxiliary variables for LMI constraints

Manuscript received May 10, 2021; revised September 23, 2021. This work was supported by the Energy Cloud R&D Program through the National Research Foundation of Korea (NRF) funded by the Ministry of Science and ICT under grant NRF-2019M3F2A1073402. (*corresponding author: Y. Kim*).

J. Park is with the Department of Convergence IT Engineering, Pohang University of Science and Technology (POSTECH), Pohang, Gyungbuk 37673, Korea.

J. Ban is with the School of Electronic Engineering, Kumoh National Institute of Technology, Gumi, Gyungbuk 39177, Korea.

Y. Kim is with the Department of Electrical Engineering, POSTECH, Pohang, Gyungbuk 37673, Korea, and also with the Institute for Convergence Research and Education in Advance Technology, Yonsei University, Seoul 03722, Korea (e-mail: powersys@postech.ac.kr).

J. P. S. Catalão is with the Faculty of Engineering of the University of Porto, 4200-465 Porto, Portugal, and also with INESC TEC, 4200-465 Porto, Portugal (e-mail: catalao@fe.up.pt).

I. INTRODUCTION

EXTREME weather events, such as floods and storms, are increasingly threatening the reliability of power grids. In the United States, the costs of weather-related power outages were estimated to be between approximately $25 billion and $70 billion per year during the period from 2003 to 2012 [1]. Over this period, the annual number of major weather-related outages, which affected at least 50,000 customers, increased from less than 40 to more than 80 [2]. Moreover, 90% of the outages occurred at the distribution level [1]–[3]. This reveals that improving the resilience of distribution networks (DNs) is of key importance when establishing future smart grids [4], [5].

Dynamic network reconfiguration (NR) has attracted much attention. This enhances the resilience by enabling self-healing operations of DNs. NR changes the topological structure of the DN through on-off operations of line switches (SWs). Faults can then be isolated, and de-energized loads are re-connected to distribution feeders that sustain load services using power supplied by a main grid and distributed generators (DGs).

In most previous studies of NR (e.g., [6]–[9]), the operational

This article has been accepted for publication in a future issue of this journal, but has not been fully edited. Content may change prior to final publication. Citation information: DOI 10.1109/TPWRS.2022.3149524, IEEE Transactions on Power Systems

schedules of SWs were determined in advance, for example, to maximize the restored load demand while minimizing the time required for load service restoration. However, switching schedules were obtained considering only the steady-state safety and operation of reconfigurable DNs, given hourly-sampled or time-invariant load demand. Further, DGs were regarded as point sources and their dynamic responses were thus neglected. Consecutive SW operations are very likely to cause sudden variations in load demand, which in turn trigger abrupt fluctuations in DN voltages in the transient state. Given the small capacities and low inertia of DGs, voltage fluctuations can cause further unexpected tripping of DGs and cascading collapse of DN voltages. This implies that it is essential to accurately reflect the dynamic responses of DGs, loads, and bus voltages into NR-aided load restoration.

In [10]–[15], the optimal NR was conducted considering the dynamics of DGs and loads and the transient operations of DNs. Specifically, in [10]–[12], the DG dynamics were reflected in optimization problems to schedule the operations of SWs, while evaluating the maximum frequency deviations due to NR. Synchronous machine-based DGs (SGs) were mainly taken into account. In [13] and [14], NR scheduling was performed with consideration of the maximum transient variations in bus voltages. The sizes and locations of de-energized loads that could be restored without violating the constraints on transient voltages were pre-selected via iterative simulation. However, load services were recovered using SGs alone, rather than SGs in cooperation with inverter-based DGs (IGs). In [15], the optimal NR was achieved for an inverter-dominated DN; the dynamics of grid-forming and grid-following IGs were reflected to estimate the frequency and voltage variations of microgrids (MGs) during NR. However, in [10]–[15], DG control was achieved mainly by conventional feedback control loops that came into effect after bus voltages had substantially deviated due to NR. Thus, current real-time voltage regulation (VR) in a reconfigurable DN can be further improved.

Only a few recent works (e.g., [16]–[18]) have investigated the coordination of DGs and SWs to improve real-time VR during load service restoration. Supplementary feedback loops were established between SGs and SWs [16] and between IGs and SWs [17], [18]. These allowed adjustment of the terminal voltages of SGs and IGs by reference to the on-off status and terminal voltages of the SWs and the currents flowing through them. The adjustments maintained the differences between the terminal voltages of each SW at zero prior to the NR; otherwise, large inrush currents were likely to occur, leading to severe voltage fluctuations. However, such supplementary control is possible only when the feeders of both terminals of the SW are energized. Thus, the method is not applicable to NR-aided load restoration, because the voltages become zero at SW terminals that are connected to interrupted loads. Consequently, the terminal voltages of SGs and IGs still need to be regulated through conventional feedback control, as in [10]–[15].

These issues have motivated the development of new strategies to regulate DN voltage deviations caused by NR preemptively, because NR is commonly performed in a controlled manner. To develop such VR strategies, the gap in the literature between studies of dynamic NR models and their application to DG control first needs to be filled. In [11] and [12], a frequency response rate (FRR) model was adopted for optimal NR considering the change in frequency dip due to a sudden load pickup. However, NR was still modeled simply as the amount of load to be restored or shed, rather than as a change in the network topology itself. This approach compromises the accuracy of estimating the dynamic responses of DGs and loads to the SW operations involved in NR-aided load restoration. The transient variations in voltages and line losses due to NR also cannot be analyzed using the FRR model. Moreover, uncertainties in the estimates of DG modeling parameters and load demands were not explicitly considered in [6]–[18]. When the uncertainties are neglected, pre-emptive regulation of DN voltages can become practically ineffective.

This paper proposes a new strategy for real-time VR of a reconfigurable, low-voltage network. Optimal feedforward control of the SGs and IGs is achieved in coordination with SW operations to preemptively mitigate transient voltage deviations at DG terminal buses caused by NR. The dynamic responses of bus voltages to NR are estimated using an analytical model of a reconfigurable network; these responses are integrated into a robust optimization problem to design optimal feedforward voltage controllers (FVCs). Uncertainties in the estimates of DG modeling parameters and load demands are considered during optimization, improving the robustness of optimal FVCs. The FVCs are incorporated in parallel with existing feedback control loops to eliminate steady-state variations in DG terminal voltages. A small-signal analysis and case studies are conducted to assess the performance of the proposed strategy.

The main contributions of this paper are summarized below:

- To the best of our knowledge, this is the first study to report feedforward control of SGs and IGs in coordination with SW operations to improve real-time VR in a reconfigurable, low-voltage network during load service restoration through NR.
- A convex optimization problem is formulated to develop the optimal robust FVCs that minimize the upcoming variations in DG terminal voltages due to NR in the sense of the H_∞ norm.
- Errors in the estimates of DG modeling parameters and load demands are reflected in the optimization problem using a polytopic uncertainty model, enhancing the effectiveness and robustness of the optimal FVCs when applied in practice.
- Comparative small-signal analysis and numerical case studies are comprehensively conducted under various grid conditions, characterized by network islanding and size, SW operations, uncertainty levels, and communications systems.

II. Fundamentals and Framework

In a reconfigurable DN, NR is conducted to isolate faults and restore loads through on-off operations of sectionalizing switches (SSWs) and tie switches (TSWs). SSWs are installed along individual feeders, and TSWs are installed between feeders. The current practices and standards [19], [20] state that a distribution system operator (DSO) should send binary signals (zero to one or vice versa) to SSWs and TSWs via communication links when changing on-off status; in this paper, the binary signals can serve as NR-initiating signals. Moreover, DGs regulate their terminal voltages to reference values in real

This article has been accepted for publication in a future issue of this journal, but has not been fully edited. Content may change prior to final publication. Citation information: DOI 10.1109/TPWRS.2022.3149524, IEEE Transactions on Power Systems

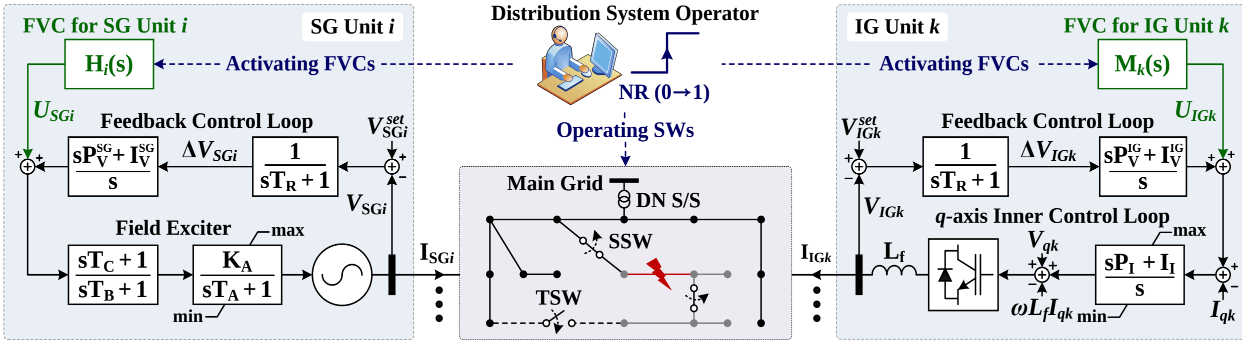

Fig. 1. Schematic diagram of the proposed strategy for real-time VR in a reconfigurable DN that includes SGs and IGs.

time, while supplying active and reactive power to distribution feeders. This facilitates the DSO to support bus voltages across a DN. Conventionally, VR has been achieved using the feedback control loops of individual DGs, commonly by employing proportional-integral (PI) controllers [21], [22]. A switching sequence can be pre-determined using various methods, for example those discussed in [6]–[9]; in this paper, for brevity, the sequence is assumed to be already available.

Fig. 1 shows a schematic diagram of the proposed VR strategy, wherein the FVCs of SGs and IGs generate reference signals for the field exciters and the *q*-axis inner control loops, respectively, in response to the binary signals (or, alternatively, the NR-initiating signals). SGs serve as grid-forming units and IGs operate as grid-following units. Note that a grid-following IG can support VR by adjusting its reactive power output [21], and the proposed strategy can also readily be applied to the grid-forming type. The FVCs are implemented in the same locations as the DGs, and incorporated in parallel with the existing feedback control loops of the DGs. The reference signals generated by the FVCs are integrated into the signals produced by the feedback loops. The FVCs enable the DGs to compensate for forthcoming variations in the DG terminal voltages caused by NR quickly and pre-emptively, allowing the feedback controllers to better attenuate remaining voltage variations. This significantly and rapidly mitigates transient voltage deviations at DG terminal buses and at load buses throughout the DN, facilitating subsequent load restorations.

In this paper, the FVCs are optimally designed using only information that is commonly available on a reconfigurable DN, SGs, and IGs. Such information is collected, updated, and accessed, for example, using advanced distribution management systems (ADMSs) [23]. In Fig. 1, $H_i(s)$ and $M_k(s)$ represent the transfer functions of the FVCs for SG unit i and IG unit k, respectively. The DSO centrally determines the optimal $H_i(s)$ and $M_k(s)$ online based on the current load demand and the locations of the target SWs to better reflect the time-varying DN dynamics, as in the multi-controller architecture [24]. The DSO then delivers $H_i(s)$ and $M_k(s)$ to the corresponding FVCs in the DG locations for localized generation of reference signals. Delivery of the NR-initiating signal and updating of $H_i(s)$ and $M_k(s)$ are performed only when SWs operations are involved. This mitigates the requirement for computation and communication systems, thus facilitating implementation of the proposed strategy in real DNs.

III. Design of Optimal Robust FVCs

A. Dynamic Responses of DG Terminal Voltages to NR

To design the proposed FVCs, the dynamic responses of the DG terminal voltages to SW operations are first estimated using an analytical model of a reconfigurable DN. In a previous study [25], a dynamic analytical model of NR was developed, wherein NR was considered to be a change in the DN topology itself. This improved the estimation accuracy of network voltage responses, compared with the conventional models in which NR was regarded simply as the load demand to be restored or shed. The previous dynamic analytical model is further adapted for application to supplementary feedforward control of DGs in response to NR-initiating signals. Briefly, the analytical model of a reconfigurable DN is represented as:

$$\Delta\dot{\mathbf{X}}_{\mathbf{DN}}(t) = \mathbf{A}_{\mathbf{DN}}\cdot\Delta\mathbf{X}_{\mathbf{DN}}(t) + \mathbf{B}_{\mathbf{DG}}\cdot\Delta\mathbf{U}_{\mathbf{FF}}(t) + \mathbf{B}_{\mathbf{NR}}\cdot u(t), \quad (1)$$

$$\Delta\mathbf{V}_{\mathbf{DG}}(t) = \mathbf{C}_{\mathbf{DG}}\cdot\Delta\mathbf{X}_{\mathbf{DN}}(t), \quad (2)$$

$$\text{where } \Delta\mathbf{X}_{\mathbf{DN}} = [\Delta\mathbf{X}_{\mathbf{SG}1}, \ldots, \Delta\mathbf{X}_{\mathbf{SG}G}, \Delta\mathbf{X}_{\mathbf{IG}1}, \ldots, \Delta\mathbf{X}_{\mathbf{IG}L}]^T, \quad (3)$$

$$\Delta\mathbf{U}_{\mathbf{FF}} = [\Delta U_{SG1}, \ldots, \Delta U_{SGG}, \Delta U_{IG1}, \ldots, \Delta U_{IGL}]^T, \quad (4)$$

$$\Delta\mathbf{V}_{\mathbf{DG}} = [\Delta V_{SG1}, \ldots, \Delta V_{SGG}, \Delta V_{IG1}, \ldots, \Delta V_{IGL}]^T. \quad (5)$$

In (1) and (2), $\Delta\mathbf{X}_{\mathbf{DN}}$ includes the state variables of the SG and IG models [see (3)]; $\Delta\mathbf{U}_{\mathbf{FF}}$ is the FVC output signals; $u(t)$ is the NR-initiating signal; and $\Delta\mathbf{V}_{\mathbf{DG}}$ is the variations in the DG terminal voltages. The corresponding coefficients $\mathbf{A}_{\mathbf{DN}}$, $\mathbf{B}_{\mathbf{DG}}$, $\mathbf{B}_{\mathbf{NR}}$, and $\mathbf{C}_{\mathbf{DG}}$ are established using linearized models of SGs, IGs, voltage-dependent loads, and distribution lines. The parameters (i.e., resistance and reactance) of distribution lines are also explicitly reflected in the coefficients and hence in the FVC models. Please refer to Appendix A for details.

In (1), $u(t)$ can represent a signal generated at any arbitrary time t without loss of generality, when $\mathbf{A}_{\mathbf{DN}}$, $\mathbf{B}_{\mathbf{DG}}$, $\mathbf{B}_{\mathbf{NR}}$, and $\mathbf{C}_{\mathbf{DG}}$ are updated prior to NR based on load demand and SW locations, as discussed in Section II. Thus, the analytical model (1)–(5) can be applied to consecutive operations of SWs. Moreover, (1)–(5) can still be used to estimate the dynamic responses of bus voltages to NR in islanded MGs [25].

B. Formulation of the Robust Optimization Problem

The proposed FVCs are designed in the form:

$$\Delta\dot{\mathbf{X}}_{\mathbf{FF}}(t) = \mathbf{A}_{\mathbf{FF}}\cdot\Delta\mathbf{X}_{\mathbf{FF}}(t) + \mathbf{B}_{\mathbf{FF}}\cdot u(t), \quad (6)$$

$$\Delta\mathbf{U}_{\mathbf{FF}}(t) = \mathbf{C}_{\mathbf{FF}}\cdot\Delta\mathbf{X}_{\mathbf{FF}}(t), \quad (7)$$

where $\Delta\mathbf{X}_{\mathbf{FF}}$ is the state variables and $\mathbf{A}_{\mathbf{FF}}$, $\mathbf{B}_{\mathbf{FF}}$, and $\mathbf{C}_{\mathbf{FF}}$ are the FVC parameters. Whereas $\Delta\mathbf{X}_{\mathbf{DN}}$ in (1) and (2) has physical variables, $\Delta\mathbf{X}_{\mathbf{FF}}$ in (6) and (7) includes only numerical variables. Thus, $\mathbf{A}_{\mathbf{FF}}$, $\mathbf{B}_{\mathbf{FF}}$, and $\mathbf{C}_{\mathbf{FF}}$ have no physical meanings.

The size of $\Delta\mathbf{X}_{\mathbf{FF}}$ is set to be the same as that of $\Delta\mathbf{X}_{\mathbf{DN}}$, so that the optimization problem for the determination of $\mathbf{A}_{\mathbf{FF}}$, $\mathbf{B}_{\mathbf{FF}}$, and,

This article has been accepted for publication in a future issue of this journal, but has not been fully edited. Content may change prior to final publication. Citation information: DOI 10.1109/TPWRS.2022.3149524, IEEE Transactions on Power Systems

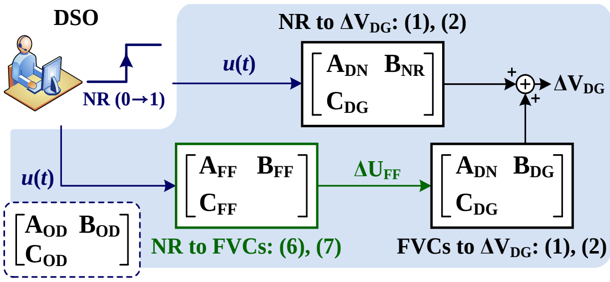

Fig. 2. Dynamic model of a reconfigurable DN with the optimal robust FVCs that are integrated with the existing feedback controllers of DGs.

C$_{\mathbf{FF}}$ can be formulated using only linear matrix inequality (LMI) constraints. Accordingly, the sizes of **A**$_{\mathbf{FF}}$, **B**$_{\mathbf{FF}}$, and **C**$_{\mathbf{FF}}$ become the same as those of **A**$_{\mathbf{DN}}$, **B**$_{\mathbf{NR}}$, and **C**$_{\mathbf{DG}}$, respectively, in (1) and (2). Moreover, in (6), the NR-initiating signal $u(t)$ serves as the common input to the FVCs, enabling preemptive compensation for voltage deviations at all DG terminal buses. Note that $u(t–T_d)$ is used, rather than $u(t)$, to analyze the effect of a communication time delay T_d on FVC performance in Sections IV and V.

The overall dynamics of the reconfigurable DN including the SGs, IGs, and corresponding FVCs are obtained by combining (1)–(7), as shown in Fig. 2. This yields the frequency-domain response $\mathbf{G}(s)$ of $\mathbf{\Delta V}_{\mathbf{DG}}(t)$ to $u(t)$, as:

$$\mathbf{G}(s) = \mathbf{C}_{\mathbf{OD}} \cdot (s\mathbf{I} - \mathbf{A}_{\mathbf{OD}})^{-1} \cdot \mathbf{B}_{\mathbf{OD}}\,, \tag{8}$$

$$\text{where } \mathbf{A}_{\mathbf{OD}} = \begin{bmatrix} \mathbf{A}_{\mathbf{DN}} & \mathbf{B}_{\mathbf{DG}} \cdot \mathbf{C}_{\mathbf{FF}} \\ \mathbf{O} & \mathbf{A}_{\mathbf{FF}} \end{bmatrix},\ \mathbf{B}_{\mathbf{OD}} = \begin{bmatrix} \mathbf{B}_{\mathbf{NR}} \\ \mathbf{B}_{\mathbf{FF}} \end{bmatrix}, \tag{9}$$

$$\mathbf{C}_{\mathbf{OD}} = \begin{bmatrix} \mathbf{C}_{\mathbf{DG}} & \mathbf{O} \end{bmatrix}. \tag{10}$$

It can be seen that **A**$_{\mathbf{FF}}$, **B**$_{\mathbf{FF}}$, and **C**$_{\mathbf{FF}}$ mainly affect $\mathbf{G}(s)$, implying that the FVCs can be optimized to minimize the forthcoming $\mathbf{\Delta V}_{\mathbf{DG}}$ due to NR. In this paper, given (8)–(10), the optimal FVC parameters (i.e., **A**$_{\mathbf{FF}}$, **B**$_{\mathbf{FF}}$, and **C**$_{\mathbf{FF}}$) are determined to minimize the maximum singular value of $\mathbf{G}(s)$ (i.e., $\|\mathbf{G}(s)\|_\infty$) by solving the optimization problem:

P$_{\mathbf{1}}$**: Problem for the design of optimal robust FVCs**

$$\underset{\mathcal{J},\,\mathcal{L}_{1\text{–}5},\,\mathcal{U}}{\operatorname{argmin}}\ \mathcal{J} \tag{11}$$

$$\text{subject to } \ \mathcal{C}_1 < 0, \tag{12}$$

$$\mathcal{C}_2 = \begin{bmatrix} \mathcal{L}_2 & \mathcal{L}_1 \\ \mathcal{L}_1 & \mathcal{L}_1 \end{bmatrix} > 0,\ \mathcal{L}_1 > 0,\ \mathcal{L}_2 > 0, \tag{13}$$

$$\mathcal{C}_3 = \begin{bmatrix} \mathcal{L}_2 - \mathcal{L}_1 & \mathcal{L}_5^T \\ \mathcal{L}_5 & \mathcal{U} \end{bmatrix} > 0 \text{ for } tr(\mathcal{U}) < \gamma, \tag{14}$$

where the element-wise expression of $\mathcal{C}_1$ in (12) is shown below. Please see Appendix B for the detailed derivation of **P**$_{\mathbf{1}}$. Briefly, in (11), $\mathcal{J}$ represents the upper bound of $\|\mathbf{G}(s)\|_\infty$, which corresponds to the peak value of the frequency response of $\mathbf{\Delta V}_{\mathbf{DG}}(t)$ to $u(t)$. Thus, **P**$_{\mathbf{1}}$ is formulated to achieve robust operation of the optimal FVCs. The constraints (12) and (13) are required to ensure bus voltage stability in the Lyapunov sense. In other words, the optimal solution (i.e., $\mathcal{J}$, $\mathcal{L}_{1\text{–}5}$, and $\mathcal{U}$) of **P**$_{\mathbf{1}}$ is obtained such that all poles of $\mathbf{G}(s)$ are located in the left-hand half plane (LHP). Moreover, (14) specifies the upper bound (i.e., γ) of the total energy of $\mathbf{\Delta U}_{\mathbf{FF}}$; this prevents excessive operation of the optimal FVCs and hence the DGs.

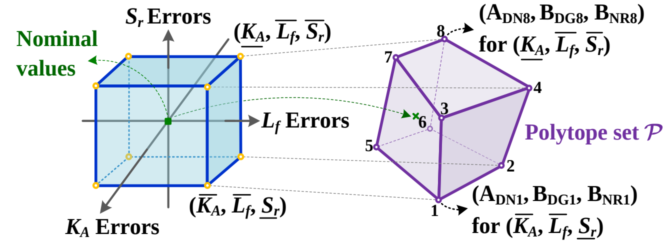

Fig. 3. Polytopic model used to estimate uncertainties in **A**$_{\mathbf{DN}}$, **B**$_{\mathbf{DG}}$, and **B**$_{\mathbf{NR}}$ for the maximum and minimum errors in the estimates of K_A, L_f, and S_r.

As shown in (11)–(15), **P**$_{\mathbf{1}}$ is a convex optimization problem with a linear objective function and LMI constraints. Therefore, **P**$_{\mathbf{1}}$ can be readily solved in real time using a common, off-the-shelf LMI solver. Given a solution of **P**$_{\mathbf{1}}$, the optimal control parameters of the FVCs are determined as:

$$\mathbf{A}_{\mathbf{FF}} = (\mathcal{L}_1\mathcal{L}_2^{-1} - \mathbf{I})^{-1}\mathcal{L}_3\mathcal{L}_2^{-1}, \tag{16}$$

$$\mathbf{B}_{\mathbf{FF}} = (\mathbf{I} - \mathcal{L}_1\mathcal{L}_2^{-1})^{-1}\mathcal{L}_4, \text{ and } \mathbf{C}_{\mathbf{FF}} = -\mathcal{L}_5\mathcal{L}_2^{-1}. \tag{17}$$

From (6) and (7), the transfer functions of the FVCs for individual SGs and IGs can then be obtained as:

$$\mathbf{G}_{\mathbf{FF}}(s) = [H_1(s), \ldots, H_G(s), M_1(s), \ldots, M_L(s)]^T, \tag{18}$$

$$= \mathbf{C}_{\mathbf{FF}} \cdot (s\mathbf{I} - \mathbf{A}_{\mathbf{FF}})^{-1} \cdot \mathbf{B}_{\mathbf{FF}}. \tag{19}$$

C. Uncertainties in the Estimates of DG and Load Parameters

As shown in (15), **P**$_{\mathbf{1}}$ is formulated using **A**$_{\mathbf{DN}}$, **B**$_{\mathbf{DG}}$, and **B**$_{\mathbf{NR}}$, which include the parameter estimates of the SGs, IGs, voltage-dependent loads, and distribution lines. Note that **C**$_{\mathbf{DG}}$ contains only ones and zeros as elements, irrelevant with uncertainty. In practice, uncertainties in parameter estimates compromise the estimation accuracies of bus voltage responses to NR and hence the performances of optimal FVCs. In [26]–[28], sensitivity analyses revealed particularly large effects of the exciter amplifier gains K_A of SGs and the filter inductances L_f of IGs on transient variations in their terminal voltages. The load demand S_r to be restored also affects the extent to which the voltages deviate in both the transient state and the steady state after NR [13], [14]. Thus, in this paper, **P**$_{\mathbf{1}}$ is extended to consider uncertainties in the estimates of K_A, L_f, and S_r, enhancing the robustness of the FVCs and their applicability in real DNs.

Specifically, the effects of uncertainties in the estimates of K_A, L_f, and S_r on **A**$_{\mathbf{DN}}$, **B**$_{\mathbf{DG}}$, and **B**$_{\mathbf{NR}}$ are first evaluated using the polytopic uncertainty model [29], shown in Fig. 3. This allows direct mapping from the error space (i.e., the blue cuboid) of K_A, L_f, and S_r to a convex polytope set $\mathcal{P}$ (i.e., the violet hexahedron) that represents a combination of **A**$_{\mathbf{DN}}$, **B**$_{\mathbf{DG}}$, and **B**$_{\mathbf{NR}}$ with parameter uncertainties. In other words, $\mathcal{P}$ is established as:

$$\mathcal{P} = Co\{[\mathbf{A}_{\mathbf{DN}1}, \mathbf{B}_{\mathbf{DG}1}, \mathbf{B}_{\mathbf{NR}1}], \ldots, [\mathbf{A}_{\mathbf{DN}V}, \mathbf{B}_{\mathbf{DG}V}, \mathbf{B}_{\mathbf{NR}V}]\}, \tag{20}$$

where $[\mathbf{A}_{\mathbf{DN}v}, \mathbf{B}_{\mathbf{DG}v}, \mathbf{B}_{\mathbf{NR}v}]$ for $v = 1, \ldots, V$ correspond to the

$$\mathcal{C}_1 = \begin{bmatrix} \mathbf{A}_{\mathbf{DN}}\mathcal{L}_2 + \mathcal{L}_2\mathbf{A}_{\mathbf{DN}}^T + \mathbf{B}_{\mathbf{DG}}\mathcal{L}_5 + \mathcal{L}_5{}^T\mathbf{B}_{\mathbf{DG}}^T & \mathbf{A}_{\mathbf{DN}}\mathcal{L}_1 + \mathcal{L}_2\mathbf{A}_{\mathbf{DN}}^T + \mathcal{L}_5{}^T\mathbf{B}_{\mathbf{DG}}^T + \mathcal{L}_3{}^T & \mathbf{B}_{\mathbf{NR}} & \mathcal{L}_2\mathbf{C}_{\mathbf{DG}}^T \\ \mathbf{A}_{\mathbf{DN}}\mathcal{L}_2 + \mathcal{L}_1\mathbf{A}_{\mathbf{DN}}^T + \mathbf{B}_{\mathbf{DG}}\mathcal{L}_5 + \mathcal{L}_3 & \mathbf{A}_{\mathbf{DN}}\mathcal{L}_1 + \mathcal{L}_1\mathbf{A}_{\mathbf{DN}}^T & \mathbf{B}_{\mathbf{NR}} + \mathcal{L}_4 & \mathcal{L}_1\mathbf{C}_{\mathbf{DG}}^T \\ \mathbf{B}_{\mathbf{NR}}^T & \mathbf{B}_{\mathbf{NR}}^T + \mathcal{L}_4^T & -\mathbf{I} & \mathbf{O} \\ \mathbf{C}_{\mathbf{DG}}\mathcal{L}_2 & \mathbf{C}_{\mathbf{DG}}\mathcal{L}_1 & \mathbf{O} & -\mathcal{J}\mathbf{I} \end{bmatrix} < 0 \tag{15}$$

This article has been accepted for publication in a future issue of this journal, but has not been fully edited. Content may change prior to final publication. Citation information: DOI 10.1109/TPWRS.2022.3149524, IEEE Transactions on Power Systems

vertices of $\mathcal{P}$. In (20), $\mathbf{A}_{\mathbf{DN}v}$, $\mathbf{B}_{\mathbf{DG}v}$, and $\mathbf{B}_{\mathbf{NR}v}$ are calculated using the maximum and minimum error percentages in the estimates of K_A, L_f, and S_r, when the DN model (1)–(5) is established.

Given the polytopic uncertainty model, the optimal FVC parameters $\mathbf{A}_{\mathbf{FF}}$, $\mathbf{B}_{\mathbf{FF}}$, and $\mathbf{C}_{\mathbf{FF}}$ are determined to minimize the H_∞ norm of $\mathbf{\Delta V}_{\mathbf{DG}}(t)$ for all inaccurate estimates of $\mathbf{A}_{\mathbf{DN}}$, $\mathbf{B}_{\mathbf{DG}}$, and $\mathbf{B}_{\mathbf{NR}}$ within $\mathcal{P}$, by solving the optimization problem:

P₂: Extension of P₁ to reflect estimation uncertainty

$$\underset{\mathcal{J},\,\mathcal{L}_{1-5},\,\mathcal{U}}{\operatorname{argmin}}\ \mathcal{J} \tag{21}$$

$$\text{subject to}\ \ \mathcal{C}_{1v} < 0\ \ \text{for}\ v = 1, \ldots, V, \tag{22}$$

$$\text{(13) and (14).} \tag{23}$$

A comparison of (12) and (22) shows that $\mathcal{C}_1$ is extended to $\mathcal{C}_{1v}$ by replacing $\mathbf{A}_{\mathbf{DN}}$, $\mathbf{B}_{\mathbf{DG}}$, and $\mathbf{B}_{\mathbf{NR}}$ in (15) with $\mathbf{A}_{\mathbf{DN}v}$, $\mathbf{B}_{\mathbf{DG}v}$, and $\mathbf{B}_{\mathbf{NR}v}$ in (20), respectively, for all v. This extension allows $\mathbf{P}_2$ to reflect all uncertainties in the estimates of K_A, L_f, and S_r within the boundary of $\mathcal{P}$, shown in Fig. 3. Consequently, the optimal solution to $\mathbf{P}_2$ and, hence, the FVCs with optimal $\mathbf{A}_{\mathbf{FF}}$, $\mathbf{B}_{\mathbf{FF}}$, and $\mathbf{C}_{\mathbf{FF}}$ can minimize the worst-case voltage variations at the DG terminals (i.e., $\|\mathbf{G}(s)\|_\infty$) for all the ranges of the uncertain estimates of K_A, L_f, and S_r [30]. The objective function and constraints on $\mathcal{C}_{2,3}$, $\mathcal{L}_{1,2}$, and $\mathcal{U}$ remain the same as in $\mathbf{P}_1$, and consequently, $\mathbf{P}_2$ remains convex. After $\mathbf{P}_2$ is solved, $H_i(s)$ and $M_k(s)$ are determined using (16)–(19), as for $\mathbf{P}_1$.

D. Practical Implementation of Optimal FVCs

Fig. 4 shows a flowchart of the proposed strategy with emphasis on the information requirements and the decision making procedures. In Steps 1–3, the DSO centrally formulates and solves $\mathbf{P}_2$, given the network-wide information and the pre-determined switching schedules. Using the optimal solution to $\mathbf{P}_2$, the DSO determines the optimal $H_i(s)$ and $M_k(s)$ of all FVCs and delivers these to the corresponding FVCs at the DG locations. The FVCs then locally generate reference signals to control the DGs, as shown in Step 4. Such hybrid control approach reduces the need for computation and communication systems, thus ensuring wide applicability of the proposed strategy to large-scale networks. Note that, for application to an islanded MG, only Step 2 needs to be adapted using the appropriate analytical model [25].

Steps 1–4 proceed within a short period of time, enabling real-time VR. In Step 1, the network-wide information and switching schedules are already available in an ADMS and can be instantly downloaded. Step 2 involves only algebraic calculations, as discussed in Appendix A, which take a short time. In Step 3, due to its convexity, $\mathbf{P}_2$ can be solved rapidly: e.g., $T_{S3} < 10$ s as discussed in Section V. Step 4 proceeds during the time when the existing feedback control loops operate to restore the DG terminal voltages back to their steady-state values in the conventional strategy. This is because, in the proposed strategy, the forthcoming voltage deviations are estimated using the analytical dynamic model of (1)–(5) wherein only the feedback control loops are applied. In [13]–[16], the feedback loops led to the transient period by up to 10 s: i.e., $T_{S4} < 10$ s.

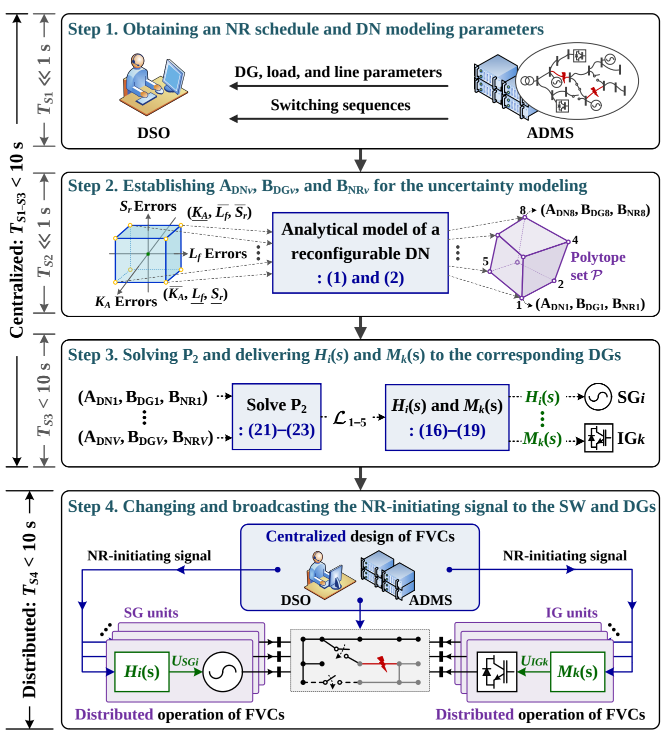

Fig. 4. A flowchart for implementation of the proposed FVCs.

IV. Small-Signal Analysis

A. Contribution of the Optimal FVCs to Real-time VR

A small-signal analysis of the proposed VR strategy was conducted with the optimal FVCs discussed in Section III. In the frequency domain, $\mathbf{G}(s)$ [i.e., (8)–(10)] was analyzed for a reconfigurable DN with the model parameters specified in Section V (see Fig. 10 and Table III). Fig. 5 shows that all eigenvalues of $\mathbf{G}(s)$ for TSW and SSW operations are placed on the LHP, confirming that the proposed strategy ensures bus voltage stability. Fig. 6 shows the singular value plots (SVPs) of $\mathbf{G}(s)$ for the proposed strategy, compared with the SVPs of

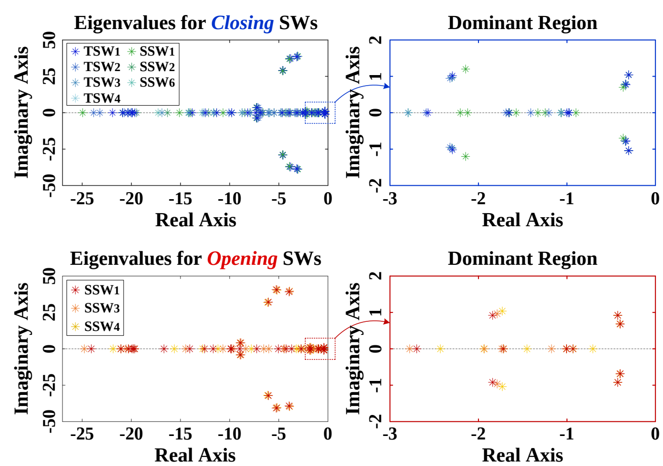

Fig. 5. Eigenvalues of $\mathbf{G}(s)$ for the proposed VR strategy.

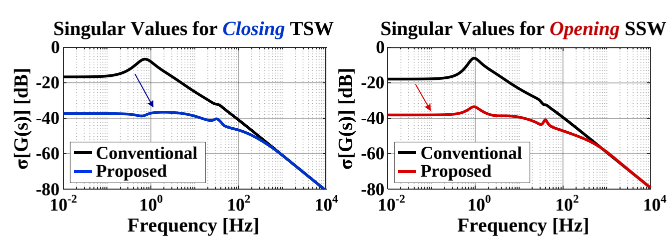

Fig. 6. Singular value plots of $\mathbf{G}(s)$ for the proposed and conventional VR strategies when a TSW and an SSW are closed and opened, respectively.

This article has been accepted for publication in a future issue of this journal, but has not been fully edited. Content may change prior to final publication. Citation information: DOI 10.1109/TPWRS.2022.3149524, IEEE Transactions on Power Systems

the conventional strategy using feedback control loops alone. The SVP comparisons demonstrate that the proposed strategy is substantially more effective in attenuating voltage deviations resulting from SW operations than the conventional strategy.

B. Sensitivity Analysis

The proposed strategy was further analyzed by considering uncertainties in the estimates of K_A, L_f, and S_r, as discussed in Section III-C. For brevity, the SGs and IGs were assumed to exhibit the same error percentages in the nominal estimates of K_A and L_f, respectively; also, the load units to be restored were assumed to exhibit the same error percentages in S_r. Fig. 7 shows the SVPs of $\mathbf{G}(s)$ in the proposed and conventional strategies when the error percentages varied by ± 30% [26], [30]. The proposed strategy still results in lower magnitudes of $\mathbf{G}(s)$ and smaller variations thereof, particularly in the frequency range below approximately 1.19 × 10^2 Hz. This verifies the robustness of the proposed strategy against large uncertainties in the estimates of the DG and load parameters.

Sensitivity analysis was also performed when the optimal FVCs responded to NR-initiating signals with a time delay of T_d. For T_d, the overall dynamics of a reconfigurable DN with the optimal FVCs are:

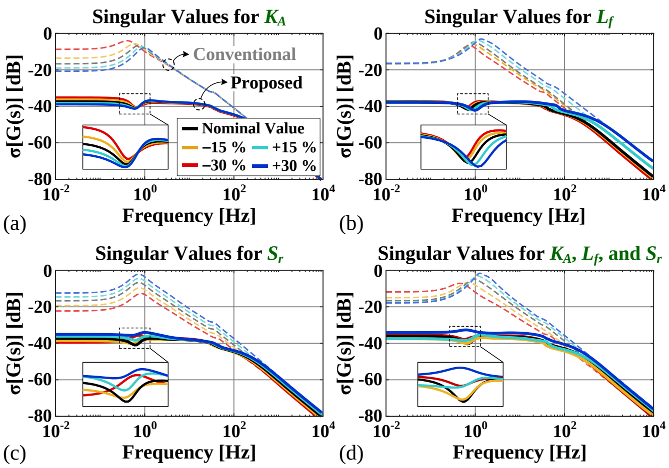

Fig. 7. The SVPs of $\mathbf{G}(s)$ for the proposed and conventional strategies with errors in the estimates of (a) K_A, (b) L_f, (c) S_r, and (d) K_A, L_f, and S_r.

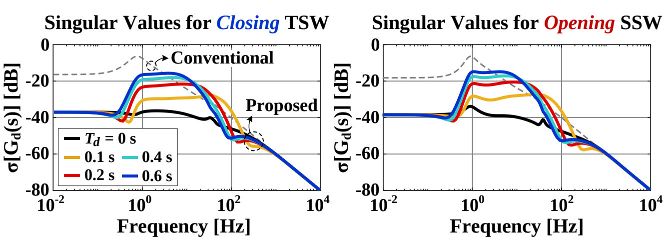

Fig. 8. The SVPs of $\mathbf{G_d}(s)$ for a communication time delay T_d.

TABLE I. COMPARISON BETWEEN THE PROPOSED AND CONVENTIONAL STRATEGIES FOR COMMUNICATION TIME DELAYS

Comparisons	Conventional	Proposed			
		T_d = 0.1 s	0.2 s	0.4 s	0.6 s
Closing a TSW					
$\|\|\mathbf{G_d}(s)\|\|_\infty$	0.464	0.038	0.079	0.121	0.159
$\|\|\mathbf{G_d}(s)\|\|_2$	0.332	0.175	0.234	0.268	0.295
Opening an SSW					
$\|\|\mathbf{G_d}(s)\|\|_\infty$	0.508	0.044	0.098	0.145	0.190
$\|\|\mathbf{G_d}(s)\|\|_2$	0.366	0.205	0.285	0.327	0.357

$$\begin{bmatrix}\Delta\dot{\mathbf{X}}_{\mathbf{DN}}(t)\\ \Delta\dot{\mathbf{X}}_{\mathbf{FF}}(t)\end{bmatrix} = \mathbf{A_{OD}}\begin{bmatrix}\Delta\mathbf{X}_{\mathbf{DN}}(t)\\ \Delta\mathbf{X}_{\mathbf{FF}}(t)\end{bmatrix} + \begin{bmatrix}\mathbf{B_{NR}}\\ \mathbf{O}\end{bmatrix}u(t) + \begin{bmatrix}\mathbf{O}\\ \mathbf{B_{FF}}\end{bmatrix}u(t-T_d). \quad (24)$$

The response of $\mathbf{\Delta V_{DG}}$ to $u(t)$ then changes from $\mathbf{G}(s)$ to:

$$\mathbf{G_d}(s) \approx \mathbf{C_{OD}}\cdot(s\mathbf{I} - \mathbf{A_{OD}})^{-1}\cdot\mathbf{d}(s), \quad (25)$$

$$\text{where}\quad \mathbf{d}(s) = \begin{bmatrix}\mathbf{B_{NR}}\\ \mathbf{O}\end{bmatrix} + \begin{bmatrix}\mathbf{O}\\ \mathbf{B_{FF}}\end{bmatrix}\cdot\left(\frac{T_d^2 s^2 - 6T_d s + 12}{T_d^2 s^2 + 6T_d s + 12}\right). \quad (26)$$

Note that the second-order Padé approximation of e^{-sT_d} was adopted in (25). Fig. 8 and Table I compare the performances of the proposed and conventional strategies when T_d increases from 0.1 to 0.6 s. Delayed FVC activations render $\mathbf{\Delta V_{DG}}$ less attenuated, particularly from about 3.53 × 10^{-2} to 3.29 × 10^2 Hz, compared to synchronous activation [i.e., $\mathbf{G}(s)$]. However, the proposed strategy still yields smaller $\|\mathbf{G_d}(s)\|_\infty$ and $\|\mathbf{G_d}(s)\|_2$ values for all T_d. In real DNs, communication time delays have been reported to be less than 0.540 s [31], confirming the practical applicability of the proposed strategy. Although it affects the transient voltage responses, T_d has no effect on voltage stability when the proposed strategy is employed because $\mathbf{d}(s)$ is stable in the bounded-input and bounded-output sense. Moreover, the eigenvalues of $(s\mathbf{I} - \mathbf{A_{OD}})^{-1}$ are the same as those of $\mathbf{G}(s)$, all of which are on the LHP (see Fig. 5).

Further sensitivity analysis was conducted when the communication systems of the DGs failed. To reflect the corresponding operations of the FVCs, (7) becomes:

$$\mathbf{\Delta U_{FF}}(t) = \mathbf{M_{FF}}\cdot\mathbf{C_{FF}}\cdot\mathbf{\Delta X_{FF}}(t), \quad (27)$$

$$\text{where}\quad \mathbf{M_{FF}} = \text{diag}(M_{SG,1}, \cdots, M_{SG,i}, \cdots, M_{SG,G}, M_{IG,1}, \cdots, M_{SG,k}, \cdots, M_{SG,L}). \quad (28)$$

In (28), $M_{SG,i}$ and $M_{IG,k}$ are binary values that indicate the communication status of SG unit i and IG unit k, respectively. The response of $\mathbf{\Delta V_{DG}}(t)$ to $u(t)$ can then be represented as:

$$\tilde{\mathbf{G}}(s) = \mathbf{C_{OD}}\cdot(s\mathbf{I} - \tilde{\mathbf{A}}_{\mathbf{OD}})^{-1}\cdot\mathbf{B_{OD}}, \quad (29)$$

$$\text{where}\quad \tilde{\mathbf{A}}_{\mathbf{OD}} = \begin{bmatrix}\mathbf{A_{DN}} & \mathbf{B_{DG}}\cdot\mathbf{M_{FF}}\cdot\mathbf{C_{FF}}\\ \mathbf{O} & \mathbf{A_{FF}}\end{bmatrix}. \quad (30)$$

Fig. 9 and Table II show the SVPs of $\tilde{\mathbf{G}}(s)$ and the corresponding numerical results under extreme conditions: i.e., when

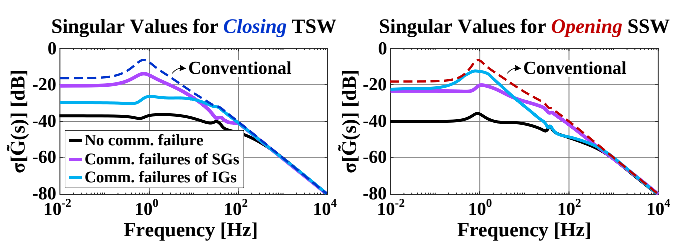

Fig. 9. The SVPs of $\tilde{\mathbf{G}}(s)$ for communication failures of the SGs and IGs.

TABLE II. COMPARISON FOR COMMUNICATION SYSTEM FAILURES

Comparisons	Conventional	Proposed		
		No failure	Comm. failures of SGs	Comm. failures of IGs
Closing a TSW				
$\|\|\tilde{\mathbf{G}}(s)\|\|_\infty$	0.464	0.012	0.391	0.068
$\|\|\tilde{\mathbf{G}}(s)\|\|_2$	0.332	0.084	0.255	0.178
Opening an SSW				
$\|\|\tilde{\mathbf{G}}(s)\|\|_\infty$	0.508	0.044	0.124	0.423
$\|\|\tilde{\mathbf{G}}(s)\|\|_2$	0.366	0.097	0.282	0.341

This article has been accepted for publication in a future issue of this journal, but has not been fully edited. Content may change prior to final publication. Citation information: DOI 10.1109/TPWRS.2022.3149524, IEEE Transactions on Power Systems

the communications of all the SGs and of all the IGs fail. This rather considerably compromises the performance of the proposed strategy. However, the proposed strategy still more effectively reduces bus voltage deviations than does the conventional strategy. Also, the extreme events have no effect on bus voltage stability when the proposed strategy is used, because the eigenvalues of $\tilde{\mathbf{A}}_{\mathbf{OD}}$ in (30) are identical to those of $\mathbf{A}_{\mathbf{OD}}$ in (9), regardless of the $\mathbf{M}_{\mathbf{FF}}$ in (28).

V. Case Studies and Simulation Results

A. *Test System and Simulation Conditions*

The proposed VR strategy was tested on the DN, modeled using the IEEE 37-bus Test Feeder [32] with modifications based on [16] and [33]. Table III lists the corresponding modeling parameters. Specifically, Fig. 10 shows the initial on-off status of SSWs and TSWs when two faults occurred at the feeders between Buses 707 and 720 and Buses 711 and 738. Moreover, the test DN contains three SGs and five IGs, with total power capacities of 1.8 and 1.0 MVA, respectively. The total load demand was 2.6 + j1.2 MVA and was distributed to the load units connected to all buses. For simplicity, the load units were assumed to have the same ZIP coefficients of 1.5, –2.3, and 1.8 for active power and of 7.4, –12, and 5.6 for reactive power. Three-phase balanced lines were also adopted with impedances set as the average value over the three phases for each line configuration.

In addition, Fig. 11 and Table IV show the self-healing

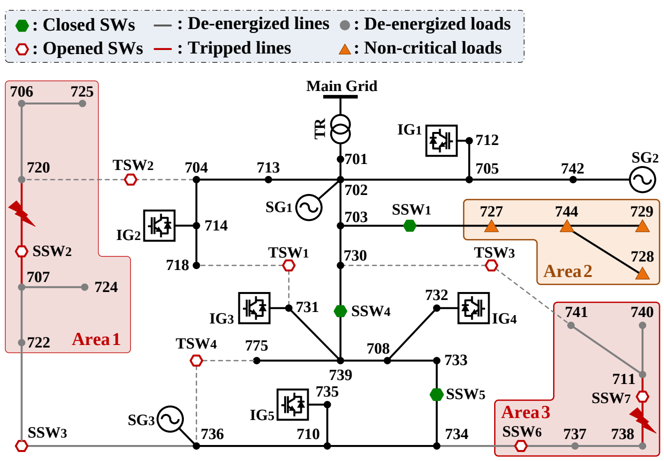

Fig. 10. Single-line diagram of the test DN.

TABLE III. Network Parameters for the Case Studies

Device	Description	Parameters	Values
SG units	nominal size and voltage	S_n [MVA], V_n [kV]	0.6, 2.4
	inertia and damping	M [s], D	0.5, 0.1
	stator reactances on the d axis	X_d, X'_d, X''_d [pu]	2.24, 0.17, 0.12
	stator reactances on the q axis	X_q, X'_q, X''_q [pu]	1.1, 0.2, 0.1, 0.04
	open-circuit time constants	T'_{qo}, T''_{qo}, T'_{do}, T''_{do} [s]	4.5, 0.1, 0.9, 0.03
	field exciter time constants	T_A, T_B, T_C, T_R [s]	0.02, 5, 1, 0.05
	voltage PI-controller gains	P_V^{SG}, I_V^{SG}	2, 4
	voltage amplifier gain	K_A	200
IG units	nominal size and DC voltage	S_n [MVA], V_{DC} [V]	0.2, 380
	filter inductance/resistance	L_f [H], R_f [Ω]	0.008, 0.91
	transducer time constants	T_R [s]	0.05
	voltage PI-controller gains	P_V^{IG}, I_V^{IG}	1, 2
	current PI-controller gains	P_I, I_I	20, 30
Loads	rated power demand	S_L [MVA]	2.6 + j1.2
	active power coefficients	p_Z, p_I, p_P	1.5, –2.3, 1.8
	reactive power coefficients	q_Z, q_I, q_P	7.4, –12, 5.6

scenario to restore de-energized loads in Areas 1 and 3. The non-critical loads in Area 2 were disconnected to support bus voltages across the DN, and then re-energized after the load restorations in Areas 1 and 3 were completed. In general, SWs are operated one at a time to prevent excessive voltage fluctuations in the transient state [13]. In this study, the time interval between SW operations was set to 10 s. For each SW operation, the optimal FVC parameters were determined within 2 s by solving $\mathbf{P_2}$ using the MATLAB toolbox YALMIP.

Furthermore, Table V lists the main features of the proposed strategy (Cases 1 and 2) and the conventional strategies (Cases 3 and 4). Cases 1 and 3 were compared to examine the effects of the optimal FVCs on real-time VR. Errors in the estimates of K_A, L_f, and S_r were not reflected in Cases 1 and 3. To allow fair comparison, Case 2 evaluated the robustness of the FVCs

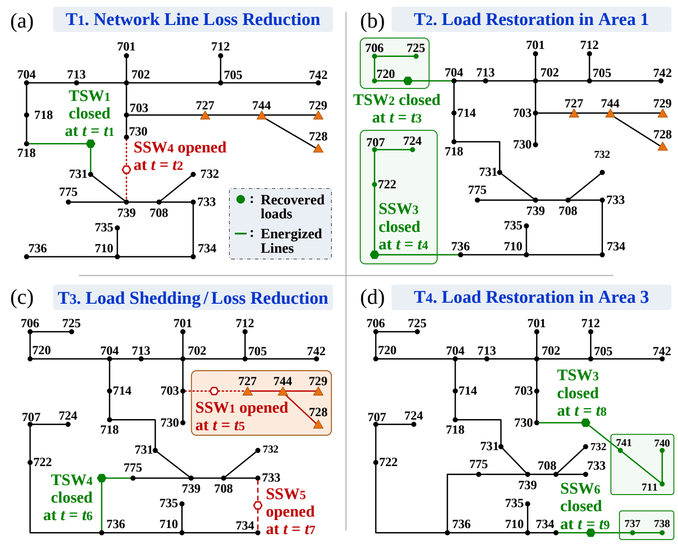

Fig. 11. Variations in the DN topology during the test self-healing scenario: (a) T_1, (b) T_2, (c) T_3, and (d) T_4.

TABLE IV. Self-Healing Scenario of the Test DN

Time periods	Operating statuses of the test DN
T_0 ($t < t_1$)	Faults occur at the feeders between Buses 707 and 720 and between Buses 711 and 738, leading to opening of TSW$_2$ and SSW$_{2,6,7}$ for isolation of the faults.
T_1 ($t_1 \le t < t_3$)	At $t = t_1$, TSW$_1$ is closed to reduce the line power losses (see Fig. 11(a)). This enables the DGs to secure additional reserve capacity for subsequent load restorations. At $t = t_2$, SSW$_4$ is opened to recover the radial structure of the DN.
T_2 ($t_3 \le t < t_5$)	TSW$_2$ and SSW$_3$ are closed at $t = t_3$ and $t = t_4$, respectively, to restore the de-energized loads in Area 1 (see Fig. 11(b)).
T_3 ($t_5 \le t < t_8$)	The non-critical loads in Area 2 are de-energized by opening SSW$_1$ at $t = t_5$ (see Fig. 11(c)), to increase the DG reserve capacity and support the DN voltages. TSW$_4$ and SSW$_5$ then operate at $t = t_6$ and $t = t_7$, respectively, to reduce line power losses, further increasing the reserve capacity.
T_4 ($t_8 \le t < t_{10}$)	TSW$_3$ and SSW$_6$ are closed at $t = t_8$ and $t = t_9$, respectively, to restore the de-energized loads in Area 3 (see Fig. 11(d)).
T_5 ($t \ge t_{10}$)	At $t = t_{10}$, SSW$_3$ is closed to restore the non-critical loads in Area 2. The self-healing operation terminates after the faults are investigated and cleared.

TABLE V. Features of the Proposed and Conventional Strategies

VR strategy		Description
Proposed	Case 1	No uncertainties in the parameter estimates
	Case 2	30% uncertainties in the parameter estimates
Conventional	Case 3	PI-based output feedback loop [21]
	Case 4	Optimal robust state feedback loop [26]

This article has been accepted for publication in a future issue of this journal, but has not been fully edited. Content may change prior to final publication. Citation information: DOI 10.1109/TPWRS.2022.3149524, IEEE Transactions on Power Systems

against errors in the parameter estimates by 30%, compared with Case 4 using the robust controller discussed in [26].

B. Performance of the Proposed VR Strategy

The proposed and conventional strategies were comparatively analyzed for the operations of TSW_2 and SSW_1 of the test DN. Fig. 12(a) shows the terminal voltages of SG_1, IG_1, and IG_2 located near TSW_2 and SSW_1. Compared with the conventional strategies, the proposed strategy significantly reduced voltage deviations caused by NR-aided load restoration and shedding. This led to a considerable reduction in the transient voltage deviations at buses where only loads were connected, as shown in Fig. 12(b). The proposed strategy also decreased the settling times of voltage deviations and hence the time required for consecutive SW operations, facilitating self-healing of the DN. For all buses, $\Delta V_{rms,avg}$, $\Delta V_{pk,max}$, and $\Delta T_{set,max}$ were estimated as:

$$\Delta V_{rms,avg} = \frac{1}{N}\sum_{n=1}^{N}\sqrt{\frac{1}{T}\sum_{t=1}^{T}\Delta V_{n,t}^2}\,,\ \Delta V_{pk,max} = \max\left(\Delta V_{pk,n}\right), \quad (31)$$

$$\text{and } \Delta T_{set,max} = \max\left(\Delta T_{set,n}\right), \quad \text{for } n = 1, \ldots, N. \quad (32)$$

Table VI shows that $\Delta V_{pk,max}$, $\Delta V_{rms,avg}$, and $\Delta T_{set,max}$ were smaller for the proposed strategy than for the conventional strategies. The improvement in VR was principally because the proposed FVCs allowed the DGs to respond to upcoming

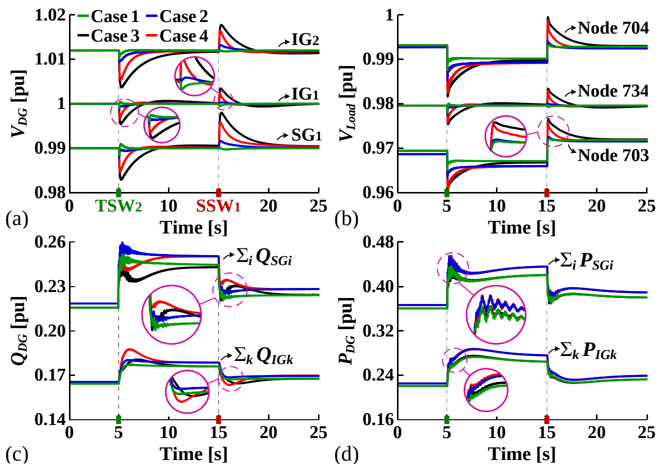

Fig. 12. Comparison of the proposed and conventional VR strategies: (a) V_{DG}, (b) V_{Load}, (c) Q_{DG}, and (d) P_{DG}.

TABLE VI. RESULTS FOR THE OPERATIONS OF TSW_2 AND SSW_1

Comparison factors		Proposed		Conventional	
		Case 1	Case 2	Case 3	Case 4
$\Delta V_{rms,avg}$	[×10^{-3} pu]	1.318	1.723	5.961	3.626
$\Delta V_{pk,max}$	[×10^{-2} pu]	0.559	0.882	1.794	1.643
$\Delta T_{set,max}$	[s]	1.667	3.371	10.823	6.172

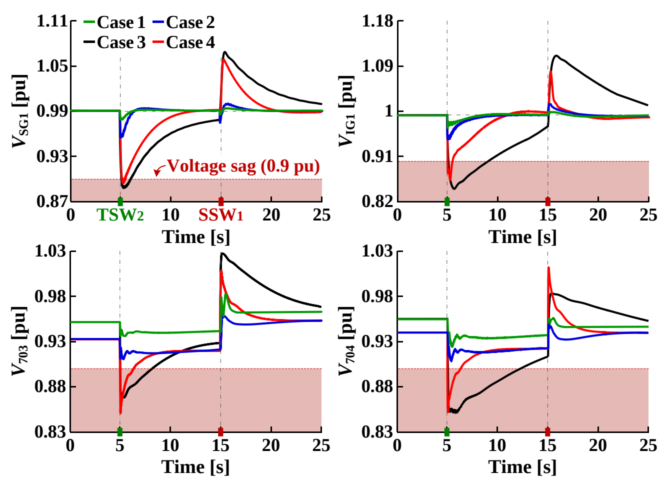

Fig. 13. Comparison of the proposed and conventional VR strategies under different operating conditions of the test DN.

TABLE VII. RESULTS FOR DIFFERENT CONDITIONS OF THE TEST DN

Comparison factors		Proposed		Conventional	
		Case 1	Case 2	Case 3	Case 4
$\Delta V_{rms,avg}$	[×10^{-2} pu]	3.506	4.639	8.434	6.961
$\Delta V_{pk,max}$	[×10^{-2} pu]	4.459	6.843	26.513	21.604
$\Delta T_{set,max}$	[s]	7.117	7.429	24.583	15.948

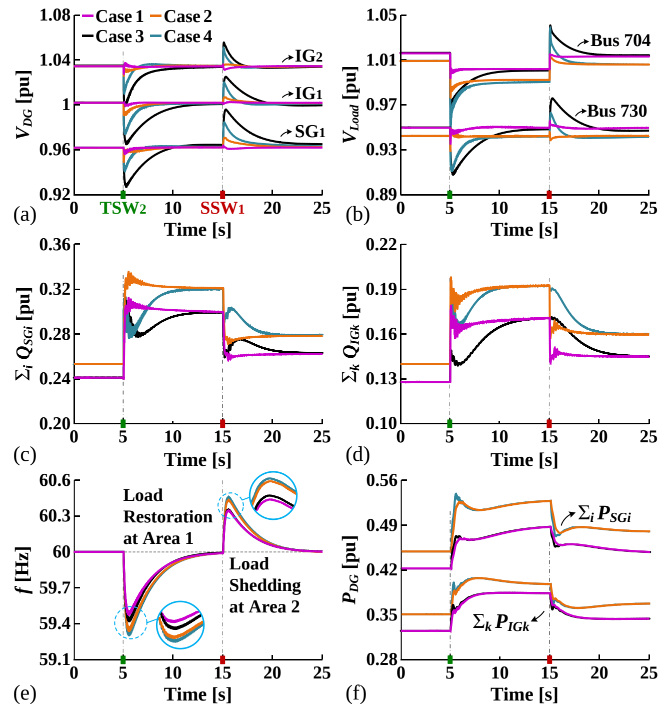

Fig. 14. Comparison of the proposed and conventional VR strategies when applied to the islanded MG: (a) V_{DG}, (b) V_{Load}, (c) Q_{SG}, (d) Q_{IG}, (e) f, and (f) P_{DG}.

TABLE VIII. RESULTS FOR THE RECONFIGURABLE, ISLANDED MG

Comparison factors		Proposed		Conventional	
		Case 1	Case 2	Case 3	Case 4
$\Delta V_{rms,avg}$	[×10^{-2} pu]	1.116	1.941	5.866	3.725
$\Delta V_{pk,max}$	[×10^{-2} pu]	2.311	3.637	10.214	9.173
$\Delta T_{set,max}$	[s]	1.939	3.813	11.672	6.941

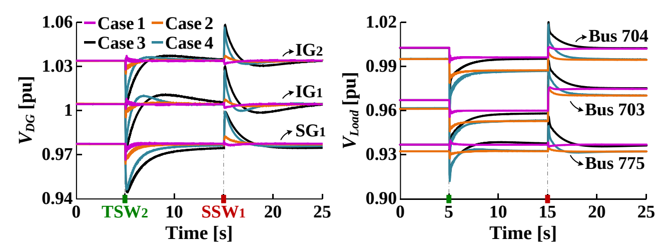

Fig. 15. Comparison of the proposed and conventional VR strategies for the case where the IGs operate as grid-forming units in the islanded MG.

TABLE IX. RESULTS FOR AN ISLANDED MG WITH GRID-FORMING IGS

Comparison factors		Proposed		Conventional	
		Case 1	Case 2	Case 3	Case 4
$\Delta V_{rms,avg}$	[×10^{-2} pu]	0.845	1.377	3.897	3.212
$\Delta V_{pk,max}$	[×10^{-2} pu]	2.021	2.858	5.927	6.188
$\Delta T_{set,max}$	[s]	1.205	2.465	13.672	4.871

This article has been accepted for publication in a future issue of this journal, but has not been fully edited. Content may change prior to final publication. Citation information: DOI 10.1109/TPWRS.2022.3149524, IEEE Transactions on Power Systems

voltage deviations caused by NR faster and more accurately (see Fig. 12(c)), including when the errors in DG parameter and load estimates were large. Fig. 12(d) shows that the active power output profiles of DGs were similar in the proposed and conventional strategies, implying that the proposed strategy can also be reliably applied to self-healing of islanded MGs.

The case studies discussed above were repeated for different conditions of the test DN. Specifically, the total load demand was increased by up to 80%, and K_A and L_f were set to 100 and 16 mH, respectively, based on the discussions in [34] and [35]. For the conventional strategies, this led to relatively large variations in the transient voltages at the DG terminal buses and hence at the load buses. For example, in Case 3, the maximum and minimum voltages were estimated to be 1.103 pu and 0.846 pu, respectively, implying that voltage stability was jeopardized. However, Fig. 13 shows that the proposed strategy maintained the transient voltage variations within an acceptable limit. Table VII also shows that $\Delta V_{rms,avg}$ and $\Delta V_{pk,max}$ were respectively 58.43% and 83.18% smaller in Case 1 than in Case 3. In Case 2, $\Delta V_{rms,avg}$ and $\Delta V_{pk,max}$ were reduced by 33.36% and 68.33%, respectively, compared to Case 4. In both Cases 1 and 2, $\Delta T_{set,max}$ was considerably smaller than in Cases 3 and 4. This confirms that the proposed strategy can adaptively reflect changes in DN operating conditions via analytical network modeling and online FVC updating, thus reducing the magnitudes and settling times of transient voltage variations.

C. Applicability to an Islanded Microgrid

Comparative case studies were conducted when the test DN was intentionally islanded from the main grid. Fig. 14 and Table VIII show that the conventional strategies led to large voltage variations in the transient state, whereas the proposed strategy successfully mitigated the transient voltage variations. This confirms that in the proposed strategy, the supplementary FVCs successfully enable the SGs and IGs to respond faster and more accurately to upcoming voltage deviations resulting from NR, regardless of whether the low-voltage network is grid-connected or islanded. Moreover, Fig. 14(e) and (f) show that the profiles of the MG frequency and DG active power were similar with each other for all Cases 1–4, confirming that the proposed strategy did not disturb MG frequency regulation.

The case studies were repeated when the IGs operated as grid-forming units in the islanded MG. The case study results, shown in Fig. 15 and Table IX, also prove the effectiveness and robustness of the proposed VR strategy in reducing the MG voltage variations in the transient state, compared to the conventional strategies. This further confirms that the proposed FVCs can adaptively reflect the dynamics of grid-forming IGs, ensuring the wide applicability of the proposed strategy, regardless of the network and IG types.

D. Performance in the Self-Healing Scenario

Additional case studies were performed to evaluate the proposed strategy with variations over time in the load demand and photovoltaic (PV) power generation [36], [37] (see Fig. 16). The optimal FVCs were developed by reference to the base load demand (i.e., $S_L = 2.6 + j1.2$ MVA). Differences between actual and base load demands were reflected as uncertainties in the network parameter estimates, in addition to uncertainties in the estimates of K_A, L_f, and S_r. Fig. 17 shows the profiles of V_{DG}, V_{Load}, Q_{DG}, and P_{DG} from T_0 to T_5 in the scenario. In Cases 1 and 2, ΔV_{DG} and ΔV_{Load} remained far lower at all times compared with Cases 3 and 4, because the optimal FVCs enabled faster and preemptive control of the DG in response to SW operations. By contrast, in the conventional strategies, DG power outputs were controlled only by the feedback loops; they came into effect after ΔV_{DG} was already significantly changed by NR. Moreover, Table X numerically compares the proposed and conventional strategies. For Case 2, $\Delta V_{rms,avg}$ and $\Delta V_{pk,max}$ were 52.3 and 51.9%, respectively, smaller than in Case 4; whereas $\Sigma_i\,\Delta Q_{SGi,rms}$ and $\Sigma_k\,\Delta Q_{IGk,rms}$ were only 4.6 and 7.6%, respectively, larger than in Case 4. This implies that the costs incurred by the increased operational stress on DGs can be adequately compensated by the savings attributable to the improved VR.

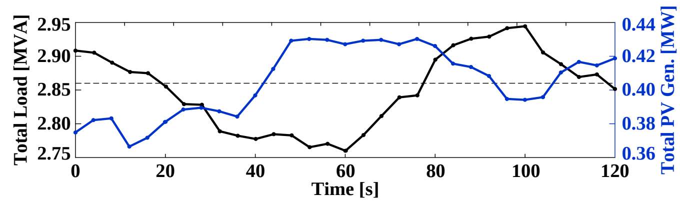

Fig. 16. Continuous variations in the load demand and PV generation.

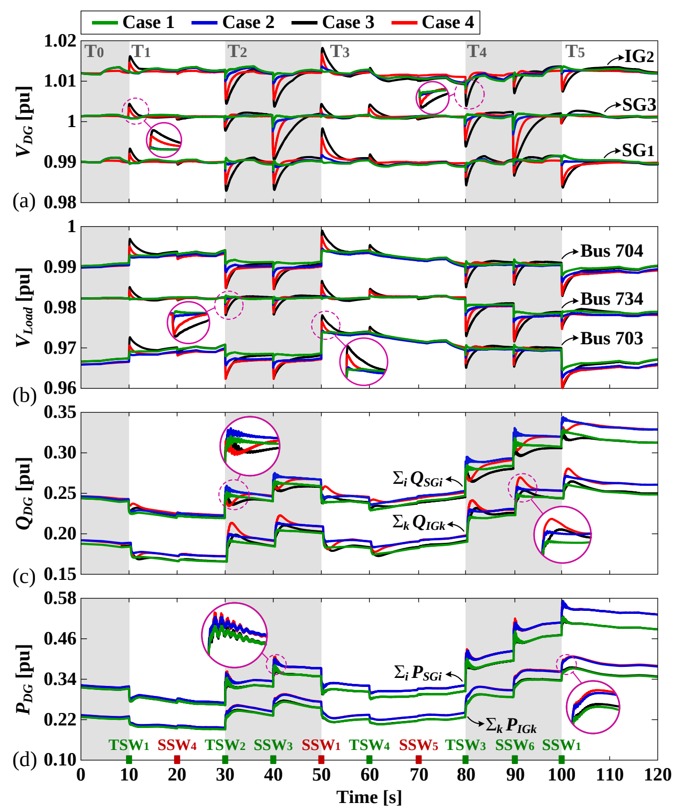

Fig. 17. Comparison of the proposed and conventional VR strategies for the self-healing scenario: (a) V_{DG}, (b) V_{Load}, (c) Q_{DG}, and (d) P_{DG}.

TABLE X. COMPARISONS FOR THE CONTINUOUS LOAD VARIATIONS

Comparison factors		Proposed		Conventional	
		Case 1	Case 2	Case 3	Case 4
$\Delta V_{rms,avg}$	[$\times 10^{-3}$ pu]	1.564	1.816	6.684	3.808
$\Delta V_{pk,max}$	[$\times 10^{-2}$ pu]	0.962	1.163	2.741	2.418
$\Sigma_i\,\Delta Q_{SGi,rms}$	[pu]	0.118	0.137	0.111	0.131
$\Sigma_k\,\Delta Q_{IGk,rms}$	[pu]	0.082	0.099	0.075	0.092

This article has been accepted for publication in a future issue of this journal, but has not been fully edited. Content may change prior to final publication. Citation information: DOI 10.1109/TPWRS.2022.3149524, IEEE Transactions on Power Systems

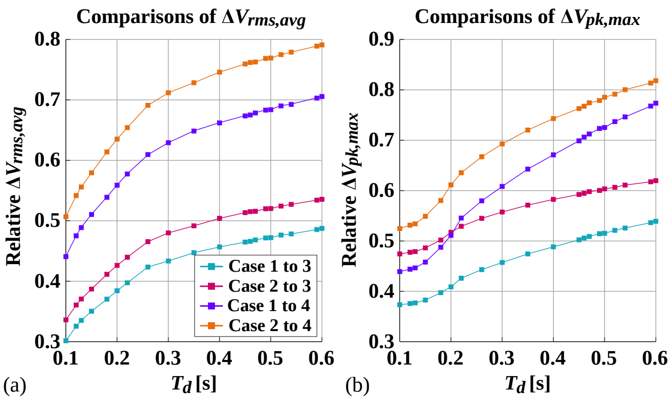

Fig. 18. The relative magnitudes of (a) $\Delta V_{rms,avg}$ and (b) $\Delta V_{pk,max}$ for different communication time delays.

TABLE XI. RESULTS FOR THE COMMUNICATION SYSTEM FAILURES

Comparison factors	Proposed: SG comm. failures	Proposed: IG comm. failures	Conventional
	Case 1		Case 3
$\Delta V_{rms,avg}$ [$\times 10^{-2}$ pu]	5.265	5.014	8.434
$\Delta V_{pk,max}$ [$\times 10^{-2}$ pu]	11.488	15.211	26.513
$\Delta T_{set,max}$ [s]	11.794	10.921	24.583
	Case 2		Case 4
$\Delta V_{rms,avg}$ [$\times 10^{-2}$ pu]	6.152	5.644	6.961
$\Delta V_{pk,max}$ [$\times 10^{-2}$ pu]	13.301	18.069	21.604
$\Delta T_{set,max}$ [s]	12.282	11.665	15.948

E. Effects of Communication Time Delays and Failures

The case studies of Section V-D were repeated to analyze the sensitivity of the proposed strategy in terms of T_d. Fig. 18(a) compares the $\Delta V_{rms,avg}$ ratios of the proposed and conventional strategies when T_d ranged from 0.1 to 0.6 s, as discussed in Section IV-B. Similarly, Fig. 18(b) shows the $\Delta V_{pk,max}$ ratios of the proposed and conventional strategies with respect to T_d. For all T_d, both the $\Delta V_{rms,avg}$ and $\Delta V_{pk,max}$ ratios remained smaller than 1.0, confirming that the proposed strategy more effectively and robustly reduced bus voltage deviations. This is also consistent with the small-signal analysis results of Fig. 8. Table XI shows that under the extreme conditions where the communications systems of all the SGs and of all the IGs failed, Cases 1 and 2 still afforded transient voltage variations of smaller magnitudes and shorter settling times than those of Cases 3 and 4, respectively.

F. Scalability Analysis

The proposed strategy was also tested on the large-scale DN, shown in Fig. 19, which was modeled based on the IEEE 123-bus Test Feeder [32]. The test DN included 12 DG units, and the DG model parameters remained the same as in Table III. It also contained 58 SSWs and 55 TSWs. Initially, three faults occurred in the DN, leading to the opening of SSW_{14}, SSW_{17}, and SSW_{22} for fault isolation. To restore the de-energized loads in Areas 1 and 2, NR was conducted in the following sequence: at t = 5 s, TSW_{28} was closed to energize the loads in Area 1; at t = 15 s, SSW_{37} was opened to disconnect the non-critical loads in Area 3; and at t = 25 s, TSW_{14} was closed to restore the loads in Area 2. Fig. 20 shows the terminal voltages of SG_2 and IG_4 located close to TSW_{14}, TSW_{28}, and SSW_{37}. Compared with the conventional strategies, the proposed strategy was more

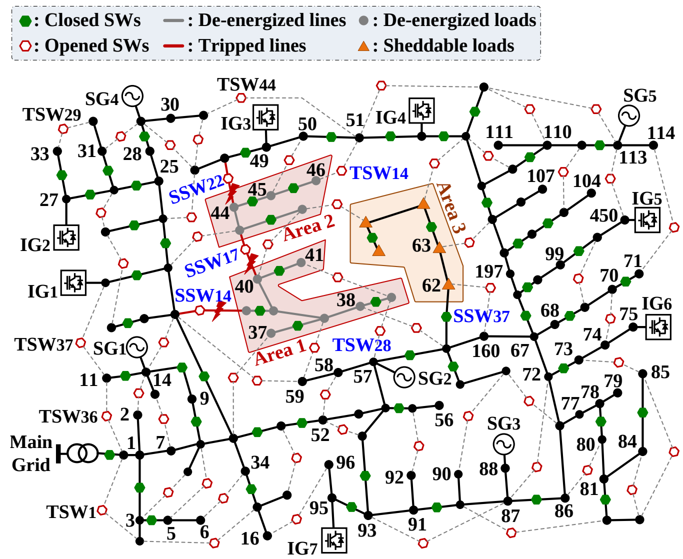

Fig. 19. Single-line diagram of the large-scale test DN.

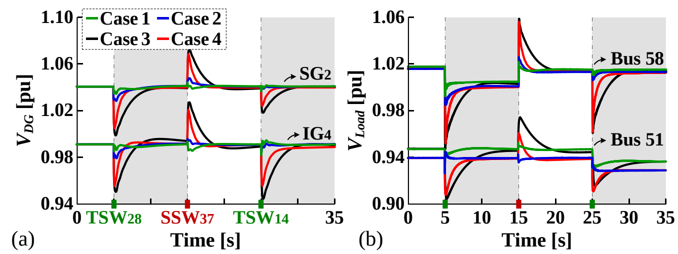

Fig. 20. Comparison of the proposed and conventional VR strategies in the large-scale DN: (a) V_{DG} and (b) V_{Load}.

TABLE XII. RESULTS FOR THE LARGE-SCALE DN

Comparison factors	Proposed: Case 1	Proposed: Case 2	Conventional: Case 3	Conventional: Case 4
$\Delta V_{rms,avg}$ [$\times 10^{-3}$ pu]	2.517	3.268	6.911	4.812
$\Delta V_{pk,max}$ [$\times 10^{-2}$ pu]	2.962	4.092	12.153	10.431
$\Delta T_{set,max}$ [s]	3.943	5.227	11.238	8.255

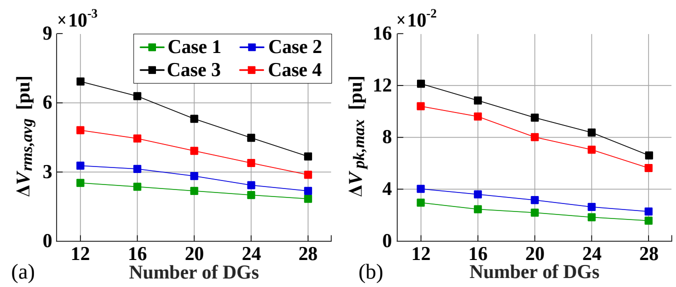

Fig. 21. (a) $\Delta V_{rms,avg}$ and (b) $\Delta V_{pk,max}$ for an increase in the total number of the DGs in the large-scale DN.

TABLE XIII. COMPUTATION TIMES TO DETERMINE THE FVC PARAMETERS

Number of DGs	12	16	20	24	28
Computation time [s]	2.708	3.633	4.724	5.957	6.875

successful in reducing the variations in the DG terminal voltages during NR. This led to significant reductions in the transient voltage deviations at Buses 51 and 58, where only loads were connected. The comparison results shown in Table XII also verify the outperformance of the proposed strategy when applied to a large-scale DN. The case studies were repeated while increasing the number of DGs from 12 to 28. Fig. 21 shows that $\Delta V_{rms,avg}$ and $\Delta V_{pk,max}$ for the proposed strategy were maintained at lower levels for all DG numbers than those

This article has been accepted for publication in a future issue of this journal, but has not been fully edited. Content may change prior to final publication. Citation information: DOI 10.1109/TPWRS.2022.3149524, IEEE Transactions on Power Systems

for the conventional strategies. Both $\Delta V_{rms,avg}$ and $\Delta V_{pk,max}$ were also gradually reduced as the number of DGs increased. Moreover, Table XIII shows that the maximum computation time to solve $\mathbf{P_2}$ increased almost linearly, rather than exponentially, with respect to the number of DGs. The results verify that the proposed strategy is readily scalable for large-scale DNs.

VI. Conclusions

This paper proposed a new VR strategy for a reconfigurable, low-voltage network wherein optimal robust FVCs enable SGs and IGs to respond faster and preemptively to real-time voltage deviations caused by NR-aided load restoration. Real-time voltage deviations at DG terminal buses were estimated using a dynamic analytical model of a reconfigurable network, and then integrated into a robust optimization problem when designing the optimal FVCs. The problem was formulated to minimize voltage deviations with respect to the H_∞ norm, while considering uncertainties in the estimates of the DG and load parameters. The results of small-signal analysis confirmed the effectiveness and robustness of the proposed strategy in terms of attenuating low-frequency components of bus voltage deviations. The case studies also revealed that the proposed strategy more effectively reduced the rms and peak-to-peak variations in bus voltages under various grid conditions, compared with conventional strategies using a PI-based feedback controller and a robust feedback controller.

Appendix

A. *Modeling a Reconfigurable Network*

The relationship between the real-time dq-axis bus voltages and injection currents in the steady-state is:

$$\mathbf{I_0} = \mathbf{Y_B}\cdot\mathbf{V_0}. \tag{A1}$$

In (A1), $\mathbf{Y_B}$ consists of block matrices, where the diagonal and off-diagonal blocks are given, respectively, by:

$$\mathbf{Y}_{\mathbf{B}jj} = \sum_{n\neq j}^{N} \mathbf{y}_{jn} \quad \text{and} \quad \mathbf{Y}_{\mathbf{B}jk} = \begin{bmatrix} -G_{jn} & B_{jn} \\ -B_{jn} & -G_{jn} \end{bmatrix}. \tag{A2}$$

In (A2), G_{jn} and B_{jn} are the real and imaginary parts of the line admittance Y_{jn} between buses j and n, respectively, as:

$$Y_{jn} = G_{jn} + j\cdot B_{jn} = 1/((R_{jn} + R_{SW}) + j\cdot X_{jn}), \tag{A3}$$

where R_{jn} and X_{jn} are the resistance and reactance, respectively, of the line between buses j and n; and R_{SW} is the SW resistance.

After NR is initiated, (A1) changes to:

$$\mathbf{I_0} + \Delta\mathbf{I}(t) = \mathbf{Y_A}\cdot(\mathbf{V_0} + \Delta\mathbf{V}(t)), \tag{A4}$$

where $\Delta\mathbf{V}(t)$ and $\Delta\mathbf{I}(t)$ are the variations in the dq-axis voltages and currents, respectively, in the transient state. From (A1) and (A4), $\Delta\mathbf{I}(t)$ can be represented as:

$$\Delta\mathbf{I}(t) = \mathbf{Y_A}\cdot\Delta\mathbf{V}(t) + \Delta\mathbf{I_T}(t), \tag{A5}$$

$$\text{where } \Delta\mathbf{I_T}(t) = \Delta\mathbf{Y}(t)\cdot\mathbf{V_0} \text{ and } \Delta\mathbf{Y}(t) = (\mathbf{Y_A} - \mathbf{Y_B})\cdot u(t). \tag{A6}$$

It can be seen from (A1)–(A6) that in the proposed strategy, an admittance matrix is established using line resistances and reactances, and NR is modeled as a discrete change in the admittance matrix (i.e., from $\mathbf{Y_B}$ to $\mathbf{Y_A}$). It leads to a step variation $\Delta\mathbf{I_T}(t)$ that arises immediately after switching operations.

In addition, considering the FVC outputs, the dynamics of the SGs and IGs can be represented in aggregated form as:

$$\Delta\dot{\mathbf{X}}_{\mathbf{DN}}(t) = \mathbf{A_X}\cdot\Delta\mathbf{X_{DN}}(t) + \mathbf{B_V}\cdot\Delta\mathbf{V}(t) + \mathbf{B_{DG}}\cdot\Delta\mathbf{U_{FF}}(t), \tag{A7}$$

$$\Delta\mathbf{I_{DG}}(t) = \mathbf{C_X}\cdot\Delta\mathbf{X_{DN}}(t) - \mathbf{D_V}\cdot\Delta\mathbf{V}(t). \tag{A8}$$

In (A7) and (A8), the coefficient matrices are block diagonal matrices, where the block matrices are established using the linearized expressions for the SG and IG dynamic models [25]. Moreover, the voltage-dependent loads can be modeled as:

$$\Delta\mathbf{I_L}(t) = \mathbf{D_L}\cdot\Delta\mathbf{V}(t), \tag{A9}$$

where $\mathbf{D_L}$ is a block diagonal matrix, the elements of which are determined based on the ZIP coefficients [25]. Using $\Delta\mathbf{I}(t) = \Delta\mathbf{I_{DG}}(t) + \Delta\mathbf{I_L}(t)$, a dynamic model of the reconfigurable DN can be established by substituting (A8) and (A9) into (A5), as:

$$\Delta\mathbf{V}(t) = \mathbf{Z}\cdot(\mathbf{C_X}\cdot\Delta\mathbf{X_{DN}}(t) - \Delta\mathbf{I_T}(t)), \tag{A10}$$

where $\mathbf{Z} = (\mathbf{Y_A} + \mathbf{D_V} - \mathbf{D_L})^{-1}$. Using (A7) and (A10), the dynamics of $\Delta\mathbf{X_{DN}}$ can then be expressed in a state-space form as:

$$\Delta\dot{\mathbf{X}}_{\mathbf{DN}}(t) = \mathbf{A_{DN}}\cdot\Delta\mathbf{X_{DN}}(t) + \mathbf{B_{DG}}\cdot\Delta\mathbf{U_{FF}}(t) + \mathbf{B_{NR}}\cdot u(t), \tag{A11}$$

where $\mathbf{A_{DN}}$ and $\mathbf{B_{NR}}$ are given, respectively, by:

$$\mathbf{A_{DN}} = \mathbf{A_X} + \mathbf{B_V}\cdot\mathbf{Z}\cdot\mathbf{C_X} \text{ and } \mathbf{B_{NR}} = -\mathbf{B_V}\cdot\mathbf{Z}\cdot(\mathbf{Y_A} - \mathbf{Y_B})\cdot\mathbf{V_0}. \tag{A12}$$

In (A11), $\mathbf{A_{DN}}$ and $\mathbf{B_{NR}}$ represent the effects of $\Delta\mathbf{X_{DN}}$ and $u(t)$ on $\Delta\dot{\mathbf{X}}_{\mathbf{DN}}$, respectively. As shown in (A12), $\mathbf{A_{DN}}$ consists of $\mathbf{A_X}$ and $\mathbf{B_V}\cdot\mathbf{Z}\cdot\mathbf{C_X}$, corresponding to the direct and indirect state-feedback effects of $\Delta\mathbf{X_{DN}}$ on $\Delta\dot{\mathbf{X}}_{\mathbf{DN}}$, respectively. In particular, $\mathbf{Z}\cdot\mathbf{C_X}$ indicates the sensitivity of $\Delta\mathbf{V}$ to $\Delta\mathbf{X_{DN}}$ [see (A10)], and $\mathbf{B_V}$ is the sensitivity of $\Delta\dot{\mathbf{X}}_{\mathbf{DN}}$ to $\Delta\mathbf{V}$. Moreover, in (A12), $\mathbf{Z}\cdot(\mathbf{Y_A} - \mathbf{Y_B})\cdot\mathbf{V_0}$ reveals the reason for the step variation in $\Delta\mathbf{V}$ due to $u(t)$, and $\mathbf{B_V}$ reflects the effect of $\Delta\mathbf{V}$ on $\Delta\dot{\mathbf{X}}_{\mathbf{DG}}$. Furthermore, $\Delta\mathbf{X_{DN}}$ in (A7) includes $\Delta\mathbf{V_{DG}} = [\Delta V_{SGi}, \Delta V_{IGk}]^T$. Thus, using $\mathbf{C_{DG}}$, $\Delta\mathbf{V_{DG}}$ can readily be extracted from $\Delta\mathbf{X_{DN}}$ as:

$$\Delta\mathbf{V_{DG}}(t) = \mathbf{C_{DG}}\cdot\Delta\mathbf{X_{DN}}(t). \tag{A13}$$

B. *Robust Optimization with LMI Constraints*

The existence of an upper bound of $\|\mathbf{G}(s)\|_\infty$ is proved as:

Lemma 1 [38]: A positive finite $\mathcal{J}$ for $\|\mathbf{G}(s)\|_\infty < \mathcal{J}$ exists if and only if there exists $\mathbf{Q} > 0$ such that

$$\mathcal{C}_\mathrm{N} = \begin{bmatrix} \mathbf{Q}\mathbf{A_{OD}} + \mathbf{A}_{\mathbf{OD}}^T\mathbf{Q} & \mathbf{Q}\mathbf{B_{OD}} & \mathbf{C}_{\mathbf{OD}}^T \\ \mathbf{B}_{\mathbf{OD}}^T\mathbf{Q} & -\mathbf{I} & \mathbf{O} \\ \mathbf{C_{OD}} & \mathbf{O} & -\mathcal{J}\mathbf{I} \end{bmatrix} < 0. \tag{B1}$$

Using ***Lemma 1***, the FVCs can be designed by solving

$\mathbf{P_N}$: Nonconvex optimization problem

$$\underset{\mathcal{J},\mathbf{A_{FF}},\mathbf{B_{FF}},\mathbf{C_{FF}},\mathbf{Q}}{\arg\min} \quad \mathcal{J} \tag{B2}$$

$$\text{subject to} \quad \mathbf{Q} > 0, \;\; \mathcal{C}_\mathrm{N} < 0 \;. \tag{B3}$$

The solution of $\mathbf{P_N}$ ensures bus voltage stability, because the Lyapunov condition (i.e., $\mathbf{Q}\mathbf{A_{OD}} + \mathbf{A}_{\mathbf{OD}}^T\mathbf{Q} < 0$) is guaranteed by $\mathcal{C}_\mathrm{N} < 0$. To convert $\mathbf{P_N}$ to a convex problem, the decision variables are replaced by the auxiliary variables $\mathcal{R}, \mathcal{N}, \mathcal{U}, \mathcal{V}$, and $\mathcal{L}_{1\text{–}5}$ for the LMI formulation. Specifically, $\mathbf{Q}$ and $\mathbf{Q}^{-1}$ are partitioned into block matrices as:

$$\mathbf{Q} = \begin{bmatrix} \mathcal{L}_1^{-1} & \mathcal{U} \\ \mathcal{U}^T & \mathcal{R} \end{bmatrix} \text{ and } \mathbf{Q}^{-1} = \begin{bmatrix} \mathcal{L}_2 & \mathcal{V} \\ \mathcal{V}^T & \mathcal{N} \end{bmatrix}, \tag{B4}$$

where all block matrices are of the size of $\mathbf{A_{DN}}$. This renders the

This article has been accepted for publication in a future issue of this journal, but has not been fully edited. Content may change prior to final publication. Citation information: DOI 10.1109/TPWRS.2022.3149524, IEEE Transactions on Power Systems

size of $\mathbf{\Delta X_{FF}}$ equal to the size of $\mathbf{\Delta X_{DN}}$. In (B4), $\mathcal{R}$, $\mathcal{N}$, $\mathcal{L}_1$, and $\mathcal{L}_2$ are positive definite matrices; $\mathcal{U}$ and $\mathcal{V}$ are arbitrary nonsingular matrices that satisfy $\mathcal{U}\mathcal{V}^T + \mathcal{L}_1^{-1}\mathcal{L}_2 = \mathbf{I}$. One can then set $\mathcal{U} = \mathcal{L}_1^{-1} - \mathcal{L}_2^{-1}$ and $\mathcal{V} = -\mathcal{L}_2$, yielding the equivalent changes of $\mathbf{A_{FF}}$, $\mathbf{B_{FF}}$, and $\mathbf{C_{FF}}$ as:

$$\begin{bmatrix} \mathbf{A_{FF}} & \mathbf{B_{FF}} \\ \mathbf{C_{FF}} & \mathbf{O} \end{bmatrix}\begin{bmatrix} \mathcal{L}_2 & \mathbf{O} \\ \mathbf{O} & \mathbf{I} \end{bmatrix} = \begin{bmatrix} (\mathcal{L}_1\mathcal{L}_2^{-1} - \mathbf{I})^{-1} & \mathbf{O} \\ \mathbf{O} & -\mathbf{I} \end{bmatrix}\begin{bmatrix} \mathcal{L}_3 & -\mathcal{L}_4 \\ \mathcal{L}_5 & \mathbf{O} \end{bmatrix}. \quad \text{(B5)}$$

In (B5), $\mathcal{L}_1\mathcal{L}_2^{-1} - \mathbf{I} = -\mathcal{L}_1\mathcal{U}$ is nonsingular, implying that $\mathbf{A_{FF}}$, $\mathbf{B_{FF}}$, and $\mathbf{C_{FF}}$ can be recovered using $\mathcal{L}_{1\text{–}5}$; see (16) and (17).

Given $\mathcal{L}_1$, $\mathcal{L}_2$, and $\mathcal{V}$, the congruence transformation is:

$$\mathcal{T} = diag(\mathcal{T}, \mathbf{I}, \mathbf{I}) \quad \text{where} \quad \mathcal{T} = \begin{bmatrix} \mathcal{L}_2 & \mathcal{L}_1 \\ \mathcal{V}^T & \mathbf{O} \end{bmatrix}. \quad \text{(B6)}$$

By applying the transformation to $\mathcal{C}_{\mathrm{N}}$ and $\mathbf{Q}$ in (B3), $\mathcal{C}_1$ in (12) and $\mathcal{C}_2$ in (13) can be obtained, respectively, as:

$$\mathcal{C}_1 = \mathcal{T}^T\mathcal{C}_{\mathrm{N}}\mathcal{T} \quad \text{and} \quad \mathcal{C}_2 = \mathcal{T}^T\mathbf{Q}\mathcal{T}. \quad \text{(B7)}$$

Considering the parameter uncertainty, $\mathcal{C}_{\mathrm{N}}$ is extended to $\mathcal{C}_{\mathrm{N}v}$ for $v = 1, \cdots, V$, and then similarly transformed to $\mathcal{C}_{1v}$ in (22) as:

$$\mathcal{C}_{1v} = \mathcal{T}^T\mathcal{C}_{\mathrm{N}v}\mathcal{T} \quad \text{for } v = 1, \ldots, V. \quad \text{(B8)}$$

Furthermore, the total energy $\mathbf{\Delta U_{FF}}(t)$ is upper-bounded by γ if the following holds [39]:

$$\mathcal{U} > \mathbf{C_{FF}}\mathcal{N}\mathbf{C}_{\mathbf{FF}}^T \quad \text{for} \quad tr(\mathcal{U}) < \gamma. \quad \text{(B9)}$$

Given $\mathbf{QQ}^{-1} = \mathbf{I}$, the relationship between the block matrices in (B4) can be specified as:

$$\mathcal{N} = -\mathcal{U}^{-1}\mathcal{L}_1^{-1}\mathcal{V} = \mathcal{L}_2(\mathcal{L}_2 - \mathcal{L}_1)^{-1}\mathcal{L}_2. \quad \text{(B10)}$$

Using (17) and (B10), (B9) is expressed in an LMI form as:

$$\mathcal{U} > \mathcal{L}_5(\mathcal{L}_2 - \mathcal{L}_1)^{-1}\mathcal{L}_5^T \quad \text{for} \quad tr(\mathcal{U}) < \gamma. \quad \text{(B11)}$$

The upper bound on the total energy of the control input can then be represented as shown in (14) by applying Schur complements to $\mathcal{U} > \mathcal{L}_5(\mathcal{L}_2 - \mathcal{L}_1)^{-1}\mathcal{L}_5^T$ in (B11).

REFERENCE

[1] R. Campbell, "Weather-related power outages and electric system resiliency," Congr. Res. Service, Washington, DC, USA, Tech. Rep. R42696, Aug. 2012.

[2] "Economic benefits of increasing electric grid resilience to weather outages," U.S. Dept. Energy's Office Elect. Energy Rel., Executive Office President, Washington, DC, USA, Tech. Rep., Aug. 2013.

[3] A. Silverstein, "Transmission 101", *NCEP Transmission Technologies Work shop*, National Association of Regulatory Utility Commissioners, Apr. 2011.

[4] *Office of the Press Secretary of the White House, Presidential Policy Directive—Critical Infrastructure Security and Resilience*.

[5] "Operates resiliently against attack and natural disaster," U.S. Dept. Energy, Nat. Energy Technol. Lab., Washington, DC, USA, Rep., 2009.

[6] C. Chen *et al*., "Resilient distribution system by microgrids formation after natural disasters," *IEEE Trans. Smart Grid*, vol. 7, no. 2, pp. 958–966, 2016.

[7] T. Ding *et al*., "A resilient microgrid formation strategy for load restoration considering master-slave distributed generators and topology reconfiguration," *Appl*. *Energy*, vol. 199, pp. 205–216, Aug. 2017.

[8] S. Poudel and A. Dubey, "Critical load restoration using distributed energy resources for resilient power distribution system," *IEEE Trans. Power Syst.*, vol. 34, no. 1, pp. 52–63, Jan. 2019.

[9] Z. Wang *et al*., "Risk-limiting load restoration for resilience enhancement with intermittent energy resources," *IEEE Trans. Smart Grid*., vol. 10, no. 3, pp. 2507–2019, May 2019.

[10] A. Golshani, W. Sun, and K. Sun, "Real-time optimized load recovery considering frequency constraints," *IEEE Trans*. *Power Syst*., vol. 34, no. 6, pp. 4204–4215, Nov. 2019.

[11] O. Bassey, K. L. Bulter-Purry, and B. Chen, "Dynamic modeling of sequential service restoration in islanded single master microgrids," *IEEE Trans. Power Syst.*, vol. 35, no. 1, pp. 202–214, Jan. 2020.

[12] B. Chen, C. Chen, J. Wang, and K. L. Bulter-Purry, "Multi-time step service restoration for advanced distribution systems and microgrids," *IEEE Trans*. *Smart Grid*, vol. 9, no. 6, pp. 6793–6805, Nov. 2018.

[13] Y. Xu *et al*., "Microgrids for service restoration to critical load in a resilient distribution system," *IEEE Trans. Smart Grid*, vol. 9, no. 1, pp. 426–437, 2018.

[14] Y. Xu *et al*., "DGs for service restoration to critical loads in a secondary network," *IEEE Trans. Smart Grid*, vol. 10, no. 1, pp. 435–447, Jan. 2019.

[15] Q. Zhang, Z. Ma, Y. Zhu, and Z. Wang, "A two-level simulation-assisted sequential distribution system restoration model with frequency dynamics constraints", *IEEE Trans. Smart Grid*, vol. 12, no. 5, pp. 3835–3846, Sep. 2021.

[16] Y. Kim, J. Wang, and X. Lu, "A framework for load service restoration using dynamic change in boundaries of advanced microgrids with synchronous-ma chine DGs," *IEEE Trans. Smart Grid,* vol. 9, no. 4, pp. 3676–3690, Jul. 2018.

[17] Y. Du, X. Lu, J. Wang, and S. Lukic, "Distributed secondary control strategy for microgrid operation with dynamic boundaries," *IEEE Trans. Smart Grid*, vol. 10, no. 5, pp. 5269–5282, Sep. 2019.

[18] Q. Zhou *et al*., "Optimal consensus-based distributed control strategy for coordinated operation of networked microgrids," *IEEE Trans. Power Syst*., vol. 35, no. 3, pp. 2452–2462, May 2020.

[19] *IEEE Standard for SCADA and Automation Systems*, IEEE Std. C37.1, 2007.

[20] *Communication networks and systems for power utility automation – Part 7-2*: *Basic information and communication structure – Abstract communication service interface* (*ACSI*), IEC Std., 2010.

[21] M. S. E. Moursi *et al*., "A dynamic master/slave reactive power-management scheme for smart grids with distributed generation," *IEEE Trans*. *Power Del*., vol. 29, no. 3, pp. 1157–1167, Jun. 2014.

[22] T. Cui *et al*., "Excitation voltage control for emergency frequency regulation of island power systems with voltage-dependent loads," *IEEE Trans. Power Syst*., vol. 31, no. 2, pp. 1204–1217, Mar. 2016.

[23] J. Wang, "Foundational report series: Advanced distribution management syste ms for grid modernization—DMS functions," Argonne Nat. Lab., Tech. Rep. ANL/ESD-15/17, Sep. 2015.

[24] D. Liberzon and A. Morse, "Basic problems in stability and design of switched systems," *IEEE Control Syst*. *Mag*., vol. 19, no. 5, pp. 59–70, Oct. 1999.

[25] J. Park, Y. Kim, and X. Lu "New analytical model of microgrid frequency and voltage variations due to network reconfiguration", *IEEE Trans*. *Smart Grid*, vol. 12, no. 1, pp. 905-908, Jan., 2021.

[26] H. Lomei *et al*., "An optimal robust excitation controller design considering the uncertainties in the excitation parameters," *IEEE Trans. Power Syst.*, vol. 32, no. 6, pp. 4171–4179, Nov. 2017.

[27] M. C. Pulcherio *et al*., "Robust stability region of a microgrid under parametric uncertainty using bialternate sum matrix approach," *IEEE Trans. Power Syst.*, vol. 33, no. 5, pp. 5553–5562, Sep. 2018.

[28] S. Leitner *et al*., "Small-signal stability analysis of an inverter-based microgrid with internal model-based controllers," *IEEE Trans. Smart Grid*, vol. 9, no. 5, pp. 5393–5402, Sep. 2018.

[29] J. C. Geromel *et al*., "On convex parametric space method for linear control design of uncertain systems," *SIAM J. Control Opt*., vol. 29, pp. 381–402, 1991.

[30] B. Zad *et al.*, "Robust voltage control algorithm incorporating model uncertain ty impacts," *IET Gener*., *Transm*. *Distrib*., vol. 13, no. 17, pp. 3921–3931, Sep. 2019.

[31] C. L. Bowen *et al*., "Next generation SCADA security: Best practices and client puzzles," in *Proc*. *6th Annu*. *IEEE SMC Information Assurance Workshop*, West Point, NY, 2005, pp. 426–427.

[32] W. H. Kersting, "Radial distribution test feeders," *IEEE Trans*. *Power Syst*., vol. 6, no. 3, pp. 975–985, Aug. 1991.

[33] D. B. Arnold *et al*., "Model-free optimal control of VAR resources in distribution systems: An extremum seeking approach," *IEEE Trans*. *Power Syst*., vol. 31, no. 5, pp. 3583–3593, Sep. 2016.

[34] A. Mitra, A. Mohapatra, S. Chakrabarti, and S. Sarkar, "Online measurement based joint estimation of synchronous generator and exciter parameters," *IEEE Trans. Energy Convers.*, vol. 36, no. 2, 820–830, Jun. 2021.

[35] X. Zhang et al., "An improved feedforward control method considering PLL dynamics to improve weak grid stability of grid-connected inverters," *IEEE Trans. Ind. Appl.*, vol. 54, no. 5, pp. 5143–5151, Sep./Oct. 2018.

[36] Fast Response Regulation Signal, PJM, Norristown, PA, USA, 2016. [Online]. Available: http://www.pjm.com/markets-and-operations/ancillaryservices/mkt -based-regulation/fast-response-regulation-signal.aspx.

[37] Y. Kim *et al*., "Analysis and experimental implementation of grid frequency re gulation using behind-the-meter batteries compensating for fast load demand v ariations," *IEEE Trans*. *Power Syst*., vol. 32, no. 1, pp. 484–498, Jan. 2017.

[38] J. G. VanAntwerp and R. D. Braatz, "A tutorial on linear and bilinear matrix inequalities," *J. Process Control*, vol. 10, no. 4, pp. 363–385, Aug. 2000.

[39] J. F. Camino and J. R. F. Arruda, "H_2 and H_∞, anfeedforward and feedback compensators for acoustic isolation," *Mech. Syst*. *Signal Process*., vol. 23, no. 8, pp. 2538–2556, Nov. 2009.

This article has been accepted for publication in a future issue of this journal, but has not been fully edited. Content may change prior to final publication. Citation information: DOI 10.1109/TPWRS.2022.3149524, IEEE Transactions on Power Systems

Jae-Young Park (Student Member, IEEE) received the B.S. degree (Hons.) in electrical engineering from Konkuk University, Seoul, South Korea, in 2015, and is currently working toward the Ph.D. degree in convergence IT engineering with the Pohang University of Science and Technology, Pohang, South Korea.

His research interests include power system reconfiguration, renewable energy resources, and grid-forming power converters.

Jaepil Ban (Member, IEEE) received the Ph.D. degree in electrical engineering from Pohang University of Science and Technology, Pohang, South Korea, in 2020. From 2020 to August 2021, He was a postdoctoral researcher with Pohang University of Science and Technology, Pohang, South Korea.

Since 2021, he has been an Assistant Professor with Kumoh National Institute of Technology. His research interests include power system control, application of reinforcement learning, and state and line parameter estimation.

Young-Jin Kim (Senior Member, IEEE) received the B.S. and M.S. degrees in electrical engineering from Seoul National University in 2007 and 2010, respectively, and the Ph.D. degree in electrical engineering from the Massachusetts Institute of Technology in 2015. He worked with Korea Electric Power Corporation as a Power Transmission and Distribution System Engineer from 2007 to 2011. He was also a Visiting Scholar with the Catalonia Institute for Energy Research in 2014, and a Postdoctoral Researcher with the Center for Energy, Environmental, and Economic Systems Analysis, Energy Systems Division, Argonne National Laboratory from 2015 to 2016.

He joined the faculty with the Pohang University of Science and Technology, where he is currently an Associate Professor with the Department of Electrical Engineering. His research fields of interest include distributed generators, renewable energy resources, and smart buildings.

João P. S. Catalão (Fellow, IEEE) received the M.Sc. degree from the Instituto Superior Técnico (IST), Lisbon, Portugal, in 2003, and the Ph.D. degree and Habilitation for Full Professor ("Agregação") from the University of Beira Interior (UBI), Covilha, Portugal, in 2007 and 2013, respectively.

Currently, he is a Professor at the Faculty of Engineering of the University of Porto (FEUP), Porto, Portugal, and Research Coordinator at INESC TEC. He was the Primary Coordinator of the EU-funded FP7 project SiNGULAR ("Smart and Sustainable Insular Electricity Grids Under Large-Scale Renewable Integration"), a 5.2-million-euro project involving 11 industry partners. His research interests include power system operations and planning, power system economics and electricity markets, distributed renewable generation, demand response, smart grid, and multi-energy carriers.